A Statistical Extended-Range Tropical Forecast Model Based on the Slow Evolution of the Madden–Julian Oscillation

DUANE E. WALISER

Institute for Terrestrial and Planetary Atmospheres, State University of New York at Stony Brook, Stony Brook, New York

CHARLES JONES

Institute for Computational Earth System Science, University of California, Santa Barbara, Santa Barbara, California

JAE-KYUNG E. SCHEMM

Climate Prediction Center, National Centers for Environmental Prediction, National Oceanographic and Atmospheric Administration, Camp Springs, Maryland

NICHOLAS E. GRAHAM

International Research Institute, Climate Research Division, Scripps Institute of Oceanography, University of California, San Diego, La Jolla, California

ABSTRACT

In this study, a statistical model is developed that exploits the slow evolution of the Madden–Julian oscillation (MJO) to predict tropical rainfall variability at long lead times (i.e., 5–20 days). The model is based on a field-to-field decomposition that uses previous and present pentads of outgoing longwave radiation (OLR; predictors) to predict future pentads of OLR (predictands). The model was developed using 30–70-day bandpassed OLR data from 1979 to 1989 and validated on data from 1990 to 1996. For the validation period, the model exhibits temporal correlations to observed bandpassed data of about 0.5–0.9 over a significant region of the Eastern Hemisphere at lead times from 5 to 20 days, after which the correlation drops rapidly with increasing lead time. Correlations against observed total anomalies are on the order of 0.3–0.5 over a smaller region of the Eastern Hemisphere.

Comparing the skill values from the above OLR-based model, along with those from an identical statistical model using reanalysis-derived 200-mb zonal wind anomalies, to the skill values of 200-mb zonal wind predictions from the National Centers for Environmental Prediction's Dynamic Extended Range Forecasts shows that the statistical models appear to perform considerably better. These results indicate that considerable advantage might be afforded from the further exploration and eventual implementation of MJO-based statistical models to augment current operational long-range forecasts in the Tropics. The comparisons also indicate that there is considerably more work to be done in achieving the likely forecast potential that dynamic models might offer if they could suitably simulate MJO variability.

1. Introduction

Useful skill in long-range weather forecasts from present-day numerical weather prediction models typically extends out to about 6 days, at which point errors associated with the initial conditions and from shortcomings in the numerical parameterization of physical processes (e.g., cumulus convection) grow to equal or exceed those from forecasts based on climatology alone (e.g., van den Dool 1994). This "6-day" timescale for useful predictability is typically determined from globally averaged rms errors or global spatial correlations between forecast and validation 500-mb height anomalies. Since most of the variations in this quantity are confined to the extratropics and because a characteristic timescale of synoptic-scale weather variability is on the order of 5 days, this 6-day limit of useful predictability is mostly a reflection of our ability to forecast midlatitude weather phenomena. However, in some cases it is reasonable to presume that the useful limit of predictability for a given phenomena is related to the timescale of the process itself (e.g., van den Dool and Saha 1990).

Corresponding author address: Dr. Duane E. Waliser, ITPA/MSRC, State University of New York at Stony Brook, Stony Brook, NY 11794-5000.
E-mail: waliser@terra.msrc.sunysb.edu

For example, the phase and strength of the quasi-biennial oscillation (QBO) would be easily predictable with reasonable skill out to 6 months or even over a year. Moreover, even at present, the evolution of the coupled ocean–atmosphere El Niño–Southern Oscillation (ENSO) phenomena is predictable with lead times of at least 6–9 months (e.g., Cane et al. 1986). While neither of these climate-related examples constitute even a rough approximation to an extremely long-range weather forecast, they each illustrate two important aspects regarding the relationship between low-frequency, quasi-predictable processes and extended-range forecasting. The first, mentioned above, is that the timescale of the process itself strongly influences the lead time through which useful predictive information can be obtained. In other words, the timescale of useful predictability is not limited to 6 days for all geophysical processes that affect weather. Second, being able to predict aspects of low-frequency processes in the ocean–atmosphere system can be extremely valuable to extended-range weather and/or short-term climate forecasting. For example, the slowly evolving state of the QBO is used as input for statistical forecasts of Atlantic hurricane activity with lead times of several months (Gray et al. 1992; Landsea et al. 1994). In addition, predictions of the state of ENSO provide valuable information on the evolution of the tropical surface boundary condition [i.e., sea surface temperatures (SSTs)], which in turn can be used to produce seasonal forecasts from an ensemble of numerical weather predictions (e.g., Ji et al. 1994; Mason et al. 1999) or from statistical models (e.g., Graham and Barnett 1995) with lead times from 1 to 12 months.

Another form of variability that evolves slowly relative to "weather" but which has yet to be fully exploited in regards to its relationship to extended-range weather forecasting is the Madden–Julian oscillation (MJO; Madden and Julian 1971). The MJO accounts for most of the variability in the tropical troposphere on intraseasonal timescales. Since its discovery in the early 1970s, a wealth of studies have been undertaken to characterize its space–time structure (see review by Madden and Julian 1994), theorize its origin (e.g., Lau and Peng 1987; Emanuel 1987; Neelin et al. 1987; Chang and Lim 1988; Hendon 1988; Wang and Rui 1990a; Salby et al. 1994; Wang and Xie 1998), and even simulate/forecast its behavior in numerical models (e.g., Hayashi and Sumi 1986; Ferranti et al. 1990; Slingo et al. 1996; Waliser et al. 1999). Observational studies have resulted in the following description. The MJO is generally characterized by an eastward propagating, equatorially trapped, wavenumber-one, baroclinic oscillation in the tropical wind field. The propagation speed is on the order of 6 m s^{-1} in the Eastern Hemisphere, where it strongly interacts/modulates deep convective activity, and about 12 m s^{-1} or greater in the Western Hemisphere, where it continues to propagate without much influence on the cloud field. Interactions

between MJO-related anomalies in convection and the large-scale circulation are strongest in the Eastern Hemisphere, over the Indian and western Pacific Oceans, where the oscillation exhibits its greatest variability and typically reaches its maximum amplitude. Such interactions strongly influence the onset and activity of the Asian–Australian monsoon system (e.g., Yasunari 1979, 1980; Hendon and Liebmann 1990a,b) and have also been shown to influence extratropical regions as well (e.g., Weickmann 1983; Liebmann and Hartman 1984; Weickmann et al. 1985; Lau and Philips 1986; Ferranti et al. 1990; Higgins and Mo 1997). Furthermore, coupling with the tropical ocean via westerly wind bursts associated with the passage of an MJO convection event can significantly modify the structure of the thermocline in the equatorial Pacific Ocean (e.g., McPhaden and Taft 1988; Kessler et al. 1996). This latter interaction has even been suggested to play an important role in triggering ENSO events (e.g., Lau and Chan 1988; Weickmann 1991; Kessler et al. 1996). Of all the above characteristics of the MJO, the most important and relevant to the present study include its very large-scale, slow eastward propagation, semioscillatory nature, strong impact on tropical rainfall in the Eastern Hemisphere, and to some extent its teleconnections to midlatitude weather.

Even with the wealth of studies undertaken on the MJO, only a few have examined the relationships between the MJO and the skill of medium-to-extended-range numerical weather forecasts, with these few generally focusing on midlatitudes or global wavenumber-one structure only. Using operational medium-range forecasts (MRF) from the National Centers for Environmental Prediction (NCEP, formerly the National Meteorological Center) for the years 1987 and 1988, Chen and Alpert (1990) showed that when the MJO amplitude is large, model forecast skill of MJO propagation and amplitude were quite good out to about 10 days based on the analysis of the 200-mb velocity potential. However, when the MJO amplitude was small, the forecast skill was poor. Similarly, Ferranti et al. (1990) demonstrated that the skill of European Centre for Medium-Range Forecasts extended-range forecasts in the extratropics are significantly improved when the errors associated with the representation of the tropical intraseasonal oscillation are minimized. Lau and Chang (1992) analyzed one season (14 December 1986–31 March 1987) of 30-day global forecasts derived from the NCEP Dynamical Extended Range Forecasts (DERFs). Their results showed that the NCEP MRF forecast model used at that time (MRF86) had significant skill in predicting the global pattern of intraseasonal variability in upper-level velocity potential and streamfunction up to 10 days, with the error growth of tropical and extratropical low-frequency modes less (greater) than persistence when the amplitude of the MJO is large (small).

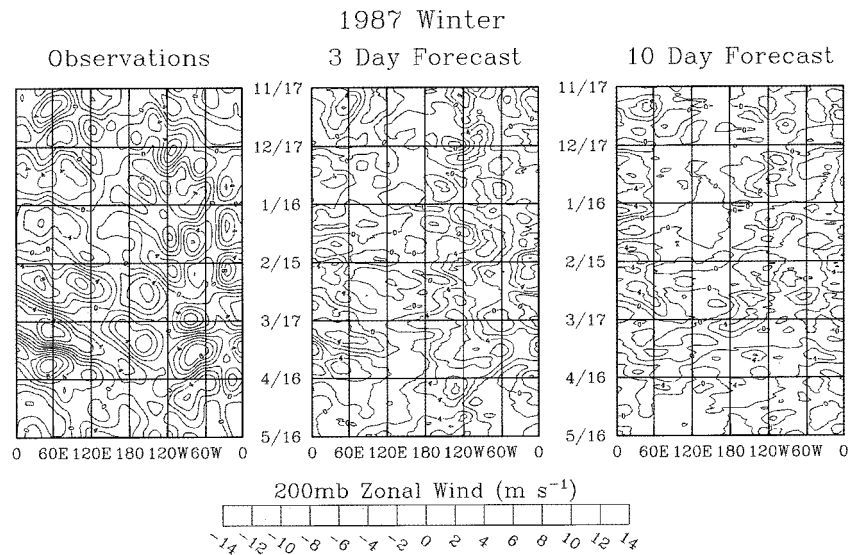A more recent version of DERF experiments has been

1987 Winter

FIG. 1. (a) 30–60-day bandpassed observations of 200-mb equatorial (7.5°N–7.5°S) zonal wind anomalies for the winter of 1987. (b) and (c) The associated 3- and 10-day bandpassed DERFs of the 200-mb equatorial zonal wind from the reanalysis version of the NCEP MRF model. See text for details concerning the bandpass procedures.

conducted with the reanalysis version (Kalnay et al. 1996) of the NCEP MRF model (Schemm et al. 1996). This experiment includes 50-day forecasts made one a day for the period January 1985–February 1990. Figure 1 shows a measure of the forecast skill for the MJO phenomena from these set of experiments. Shown in the left panel of the figure are 30–70-day bandpassed observations of 200-mb equatorial zonal wind[1] anomalies for the winter of 1987, an especially active period for the MJO (Salby and Hendon 1994). The observations show four distinct intraseasonal "oscillations" during this period in which the 200-mb zonal wind anomalies vary up to ±10 m s⁻¹ and propagate from the eastern Atlantic sector to the western Pacific at about 6 m s⁻¹, weaken as they progress to the date line, and then continue to propagate eastward at a speed of about 20 m s⁻¹. Shown in the middle and right panels are the associated 3- and 10-day bandpassed forecasts of the 200-mb equatorial zonal wind. The bandpass filtering for the observations as well as the forecasts was performed using an iterative moving-average procedure (Brooks and Carruthers 1953). For the observations, the filtering was performed on a 60-month (January 1985–December

1989) daily time series at each grid point. For the forecasts, the filtering was performed separately on each 50-day forecast of the same 60-month period at each grid point. The procedure is applied in the following way. In order to remove variations longer than 70 days, a moving average of length equal to 25 days is applied four times to each segment of 50-day forecasts (each filtered time series becomes the input for the next pass and so on). The smoothed time series obtained this way is subtracted from the original 50-day forecasts to provide a time series containing variations less than 70 days. Next, a moving average of length 9 is applied four times to remove variations less than 30 days. Since each of the above moving average filters requires additional points at the ends of the 50-day forecasts (12 and 4 data points at each end, for each filter, respectively), an autoregressive model of order 10 is fit to the 50-day forecasts at each pass of the moving average to generate the additional points (see Jones et al. 1999, manuscript submitted to *Climate Dyn.* for further details). Note that since the filtering is performed on each forecast separately, the data presented in the forecast panels are not continuous in the strictest sense and this introduces the high-frequency variability evident in these two panels. The 3-day forecast data show modest resemblance to the observations, with the best agreement occurring in the longitude range 0°–150°E, with rather poor agreement at other longitudes. The time period of best agreement occurs between the middle of January and the middle of April when the 200-mb zonal wind variations are strongest in the observations. During this period, the 3-day forecast does a reasonably good job at forecasting the evolution of the zonal wind. At 10 days, there is

---

[1] Due to the vast amount of data produced by this DERF experiment, only a subset of variables (200-mb winds, 500-mb heights, 850-mb winds and temperature, and precipitation) were saved in a manner that made them readily accessible. Of these variables, 200- and 850-mb zonal winds and precipitation typically provide the best measures of tropical intraseasonal variability, and of these variables, it was thought that the 200-mb zonal winds would be modeled more favorably by the MRF model and thus be the best variable for the present analysis.
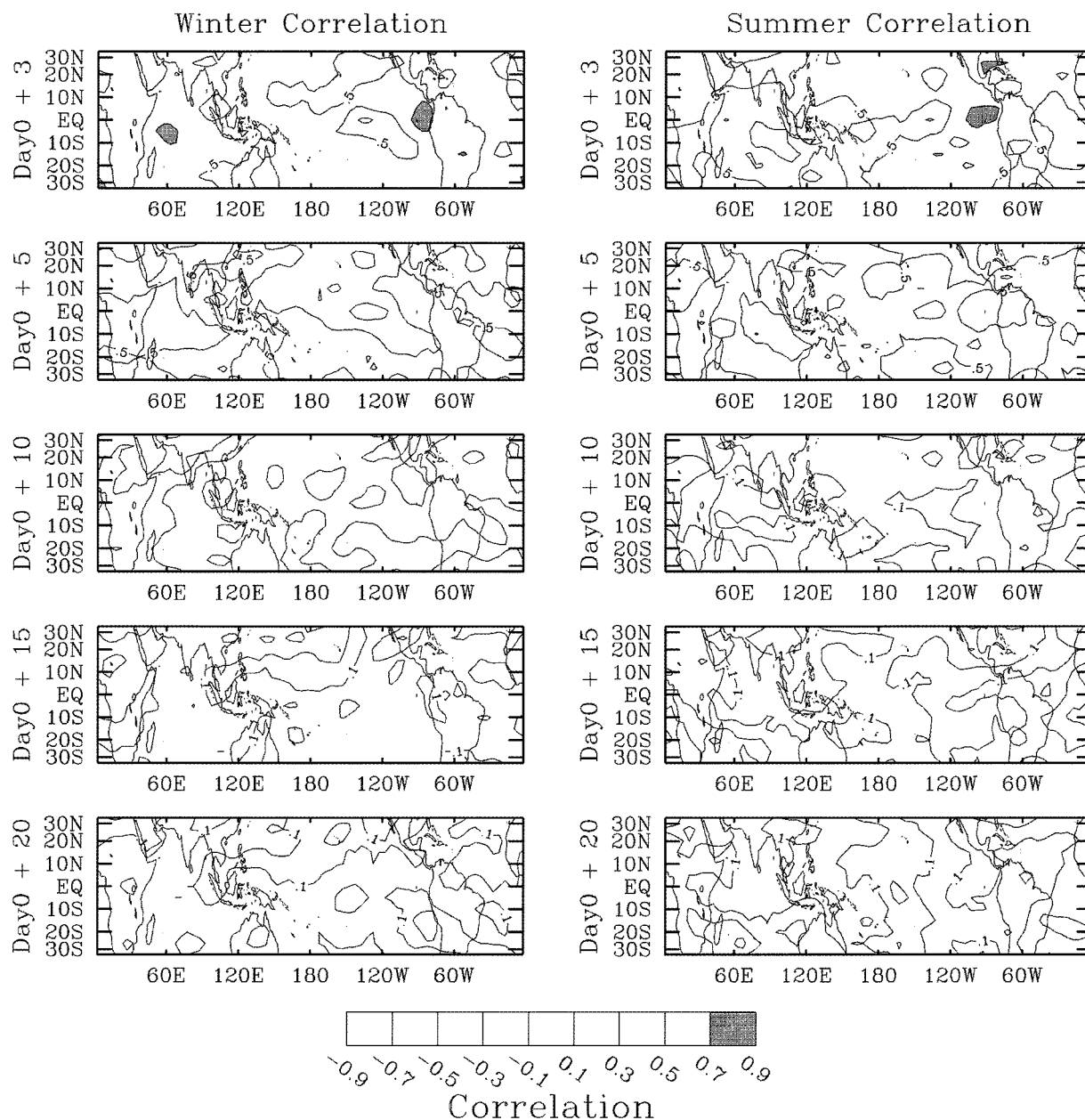
FIG. 2. Temporal correlations between bandpassed observations of 200-mb zonal winds and the associated bandpassed values from the NCEP DERFs for winter (left) and summer (right) seasons for the entire 61-month DERF experiment period. The plots show correlations for 3-, 5-, 10-, 15-, and 20-day forecasts, represented here as "Day0 + 3," "Day0 + 5," etc.

still some evidence of the two strongest eastward prop-agating events, although by this time the overall mag-nitude of the intraseasonal variability is considerably diminished.

Figure 2 shows a quantitative measure of forecast skill for the MRF model in predicting tropical intraseasonal variations. Temporal correlations are shown between predicted and observed bandpassed 200-mb zonal wind anomalies versus forecast day for the global tropical

region for the entire 61-month experiment period. For these calculations, the data were separated into winter (1 November–31 March) and summer (1 May–30 Sep-tember) periods. Evident is the rapid decline of forecast skill in the first few days, from about 0.3 to 0.5 at forecast day 5 to about 0.1 to 0.3 at forecast day 10. These values suggest little if any predictive value be-yond about 5 days. While this timescale is not signifi-cantly different from the more generic 6-day timescale

associated with global weather forecasts discussed above, the fact that it applies to a fairly well-defined phenomena with an intraseasonal timescale (i.e., 30–60-day MJO) indicates that the MRF model is likely not performing up to the potential skill level that a dynamical forecast might be expected to possess for such a slowly evolving phenomena. This does not come as a significant surprise. The skill of numerical weather forecasts in the Tropics have always tended to lag that in the midlatitudes (e.g., Kanamitsu 1985; Reynolds et al. 1994). This reduced skill is due to the greater prevalence of cumulus convection in the Tropics, a process extremely difficult to parameterize, and due to the lack of a simple force balance (e.g., quasigeostrophic). In the Tropics, the pressure gradient and Coriolis forces are weaker, and thus boundary layer friction and transients play a relatively larger role in the force balance.

The above state of affairs regarding dynamical forecasts of tropical intraseasonal variability raises two questions. The first is, how skillful should we expect such forecasts to be? The second is, how well might statistical models perform at the same task? Fortuitously, answering the second question may help us constrain and/or provide the answer to the first question. Further, if the answer to the second question is encouraging, then statistical models especially formulated to capture and predict the evolution of intraseasonal variability might help augment current operational extended-range forecast procedures until the skill of the numerical model meets or exceeds that from the statistical models. To help answers the above two questions, we have developed a statistical model to begin exploring the feasibility of applying such models to the prediction of tropical intraseasonal variability. Although not new, this idea has received little attention. Von Storch and Xu (1990) examined principal oscillating patterns (POPs) of tropical 200-mb velocity potential anomalies from a 2-yr subinterval of a 5-yr dataset. Upon verifying against the remaining 3 years of data, they found that forecasts based on the first pair of POPs produced forecasts that were better than persistence and appeared to have useful skill out to at least 10 days. While theirs is a very encouraging result, the extremely limited length of data used combined with the nonstationary characteristic of the MJO over interannual timescales (e.g., Salby and Hendon 1994) still warrants caution in assessing the applicability of their result. Moreover, 200-mb velocity potential is a very smoothly varying quantity and one that is only loosely related to near-surface meteorological variables of interest (e.g., precipitation); thus it is not clear if much practical value can be afforded from their result. More recently, Kousky and Kayano (1993) suggested that real-time monitoring of the MJO could be achieved by projecting anomalies of a number of fields [e.g., outgoing longwave radiation (OLR), 200-mb velocity potential, surface pressure, etc.] onto their principal combined extended empirical orthogonal function patterns that would indicate the present phase and strength of the MJO in the tropical atmosphere and its likely evolution. In this paper, we build on these earlier studies to further address the two questions posed above. In doing so, we use slightly different statistical techniques along with considerably more data for model development and validation, and provide a more direct comparison between our statistical model and a present-day numerical counterpart. In the next section, we describe the statistical model and the datasets used. In section 3, we present the model validation results. In section 4, we summarize our results, discuss the model's limitations, compare results from a version of the same statistical model based on 200-mb zonal winds to the DERF figures shown above, and discuss plans for future work.

2. Model specifics

Most of the results presented in this paper are based on a statistical model that utilizes anomalies of OLR (Gruber and Krueger 1984) as both predictors and predictands. The choice of OLR as a predictand is based on our desire for a forecast state that has a fairly tangible relationship to rainfall. In contrast to 200-mb winds or velocity potential, which are only loosely related to rainfall, OLR anomalies have been used in numerous studies as a surrogate for tropical rainfall anomalies due to their close association with anomalies in tropical deep convection. These studies include analysis of the ENSO phenomena (e.g., Gill and Rasmusson 1983; Rasmusson and Wallace 1983; Lau and Chan 1988); the relationships between large-scale characteristics of convection, SST, and wind (e.g., Graham and Barnett 1987; Gutzler and Wood 1990; Waliser and Graham 1993); as well as tropical climate trends (e.g., Nitta and Yamada 1989; Graham 1995; Morrissey and Graham 1996; Waliser and Zhou 1997). Even more relevant to the present study is the use of OLR for studying intraseasonal variability (e.g., Weickmann 1983; Weickmann et al. 1985; Lau and Chan 1985, 1986, 1988; Knutson and Weickmann 1987; Wang and Rui 1990b; Salby and Hendon 1994; Hendon and Salby 1994; Hendon and Glick 1997; Jones et al. 1998) and for producing actual estimates of tropical rainfall (e.g., Morrissey 1986; Yoo and Carton 1988; Arkin and Ardanuy 1989; Janowiak and Arkin 1991; Xie and Arkin 1997). Additional discussion of the uses of OLR along with a comparison between OLR and other satellite-derived measures of tropical deep convection can be found in Waliser et al. (1993).

While the presentation mainly focuses on the OLR-based model, statistical models using other variables or their combinations have been examined as well. These are discussed in the section 4, and in fact a model using 200-mb zonal winds in a fashion identical to that described below is introduced briefly for the purposes of providing a direct comparison with the numerical forecasts presented in the introduction. For the OLR-based model, 5-day average (pentad) OLR data were obtained

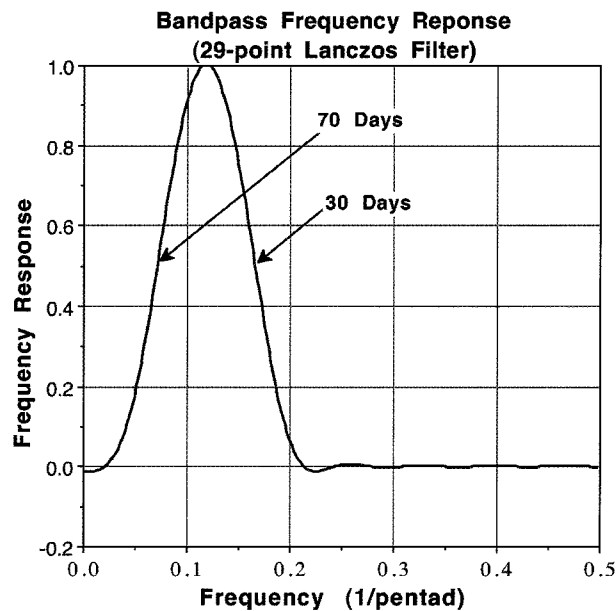**Bandpass Frequency Reponse**
(29-point Lanczos Filter)

FIG. 3. Spectral response of the 29-point Lanczos bandpass filter applied to the OLR pentad data.

from NCEP for the years 1979–96. These data have 2.5° spatial resolution and contain exactly 73 pentads for each year. In the case of leap years, the extra day (i.e., 29 February) is included in the pentad extending from 25 February to 1 March. For this study, only the data between 30°N and 30°S are used. To reduce the computation expense for the exploratory phase of this work, the data resolution was reduced to 5° × 5°. In order to focus the model's skill on the intraseasonal timescale, the data are bandpassed with a 30–70-day Lanczos bandpass filter (Duchon 1979). The spectral response function of the filter is shown in Fig. 3. The filtering is done in frequency space by applying a Fourier transform to the time series at each grid point, windowing the resulting complex spectral coefficients by the function in Fig. 3, and then performing an inverse Fourier transform.

Predictors for the model are made up of the two "most recent" bandpassed OLR pentad maps (concatenated together). For example, for any pentad T_N, the associated predictors would be the pentad maps T_{N-1} together with T_N. Predictands for the model are "future" bandpassed OLR pentad maps, with lead times of 1–9 pentads (i.e., 5, 10, . . . , 45 days). Thus, for the predictor composed of pentads T_{N-1} and T_N, the predictands would be the single pentads $T_{N+1}, . . . , T_{N+9}$. For each of the nine lead times, a singular value decomposition (SVD; see Bretherton et al. 1992) between all the predictor sets and their associated predictands at the given lead time is performed. The output from this procedure provides a set of "modes," one set for each lead time, that provide a way of mapping an input predictor (i.e., past and present "rainfall") to the most likely output predictand (i.e., future rainfall).

The SVD procedure described above was performed on the first 11 years of data (1979–89). Before the decomposition, the data/models were also separated into northern summer (16 May–16 November) and northern winter (17 November–15 May) due to the differences in the nature of the intraseasonal variability between these two periods (e.g., Wang and Rui 1990b; Salby and Hendon 1994). Hereafter, these two periods will be referred to as "winter" and "summer," and the half-year they each encompass will be referred to as a "season." In the end, the above procedure produces two separate statistical models, one for summer and one for winter, for each different lead time.

The leading modes of the prediction models illustrate many of the well-known features of the MJO and its evolution. For example, the variability contained within the first few modes is focused over the Indian and western Pacific Oceans, and the first two modes illustrate the general eastward progression of anomalous rainfall patterns over this same region. These characteristics can be seen in Figs. 4 and 5, which show the first two modes for a prediction of the third pentad in the future (i.e., denoted "Pentad0 + 3") for winter and summer, respectively. Immediately evident is the relatively high concentration of variability in the Eastern Hemisphere for each of the modes shown, with some tendency for the variability to be further concentrated near the equator. The eastward propagation is mildly evident within a single mode's progression from its Pentad0 − 1 (previous pentad) to Pentad0 (present pentad) representations, and then markedly obvious when examining the change that is projected to occur for the forecast time, Pentad0 + 3.

The spatial relationships between the mode-1 and -2 patterns tend to be in quadrature, which when combined ends up producing the oscillatory/migratory nature of the phenomena. Similar quadrature relations can be found in the empirical orthogonal function decompositions of OLR by Murakami (1979), Lau and Chan (1988), and Ferranti et al. (1990). The main differences between the summer and winter patterns is the tendency for the convective signal to move southward along the South Pacific convergence zone (SPCZ) in the winter patterns, and northward into India and southeast Asia in the summer patterns (cf. Wang and Rui 1990b). The mode-1 and mode-2 patterns for other lead times primarily differ in the phase lag between the predictor patterns and their associated predictand pattern, with the phase lag of the eastward moving "wave" increasing for longer lead times. Figure 6 shows the mode-3 patterns for both winter (left) and summer (right). Similar to modes 1 and 2, the patterns for mode 3 tends to migrate south in the winter and north in the summer. In contrast to modes 1 and 2, the spatial patterns exhibit smaller scales of variability, with three rather than two regions of extrema (i.e., "nodes"). Furthermore, the mode-3 patterns exhibit an asymmetric rather than a symmetric wavelike pattern about the equator.
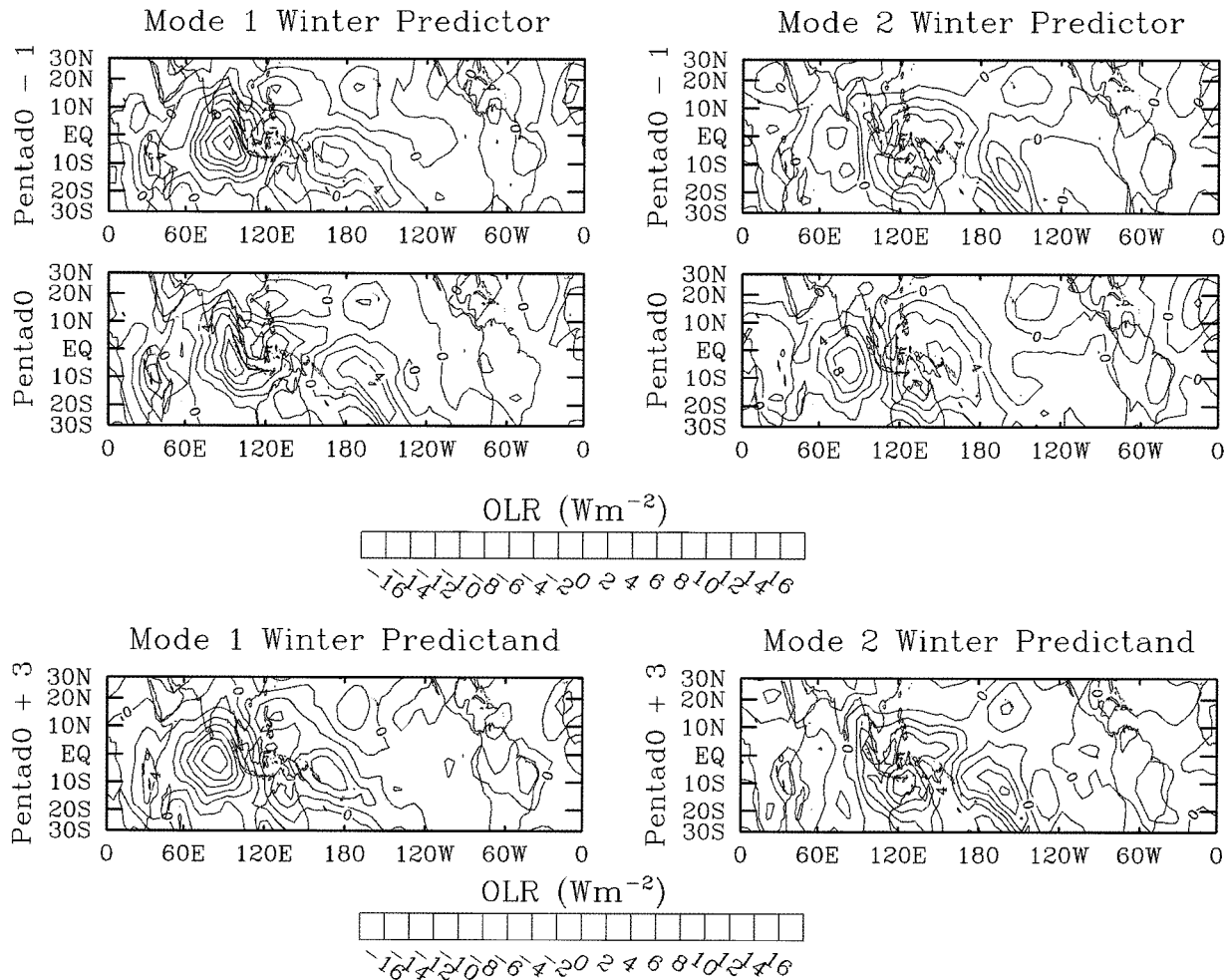
FIG. 4. Modes 1 and 2 for Northern Hemisphere "winter" 3-pentad lead forecast. The top panels show the predictor patterns for Pentad0 (the current pentad) and Pentad0 − 1 (the previous pentad). The bottom panels show the associated predictand patterns for Pentad0 + 3 (i.e., 3 pentads in the future). See text for a definition of winter and a description of the model development period used.

The forecast models, one for each lead time and season, are made up of the above subset of modes obtained from the SVD analysis. The left panels of Fig. 7 show the fractional covariances accounted for by the first 10 modes for both summer and winter for lead times of 1, 4, and 8 pentads, along with an estimate of their statistical significance. The plots demonstrate three features. First, a significant fraction of the covariance between the predictor and predictand datasets is contained within the first two modes for any given lead time. Specifically, the fractional covariances of modes 1 and 2, for the lead times shown, generally lie between 24%–37% and 18%–28%, respectively, with the percentages being less for longer lead times. Percentages for higher modes generally contain on the order of 11% or less, with percentages at longer leads increasing slightly for the higher modes. Second, for all the modes shown, there are only modest differences in the covariance percentages between summer and winter and/or between

different lead times, even though the spatial patterns differ quite substantially (i.e., Figs. 4 and 5). Third, given the 99% significance level shown, at least the first three modes in each case can be judged as statistically significant; this is also true for all the lead times for both summer and winter seasons.

The right panels of Fig. 7 convey similar information except in terms of the fractional variances of the predictand field accounted for by the first 10 modes for both summer and winter for lead times of 1, 4, and 8 pentads, along with an estimate of their statistical significance. These percentages provide information about the amount of filtered variance that can be expected to be accounted for by the model. The plots show that the first two modes account for about 12% and 10%, respectively. The percentages of the remaining modes diminish fairly rapidly with the first few remaining above the 99% signficance level.
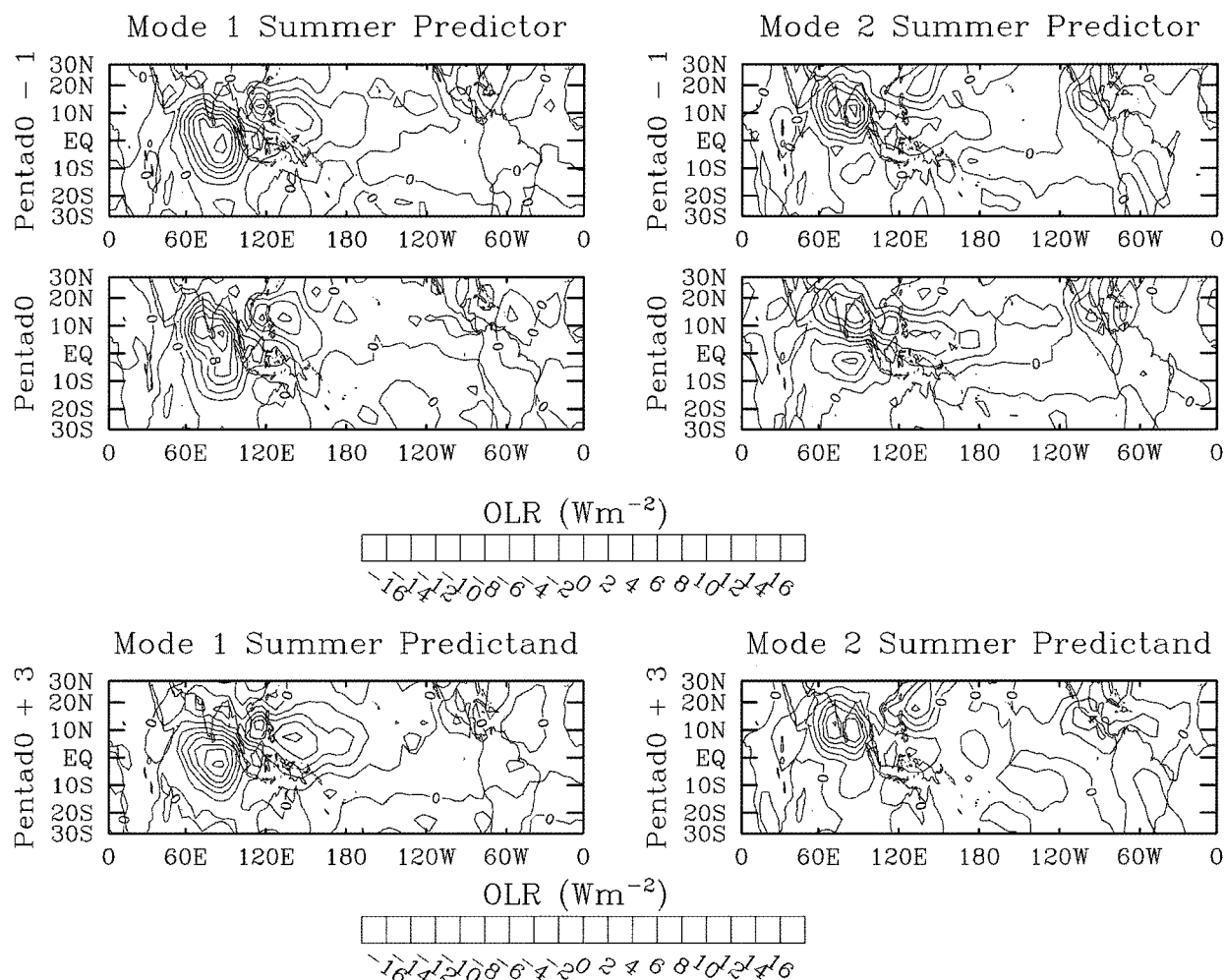
The 99% significance level presented in Fig. 7 was

FIG. 5. Same as Fig. 4, except for Northern Hemisphere summer.

obtained as follows. First, the decorrelation scales in time, and with latitude and longitude, were determined for the bandpassed input data. These were approximately 6 pentads, 10° latitude, and 20° longitude. The predictor and predictand datasets for winter and summer for a 1-pentad lag were then subsampled by these values so that each grid value represented an independent sample. Thus instead of 692 pentads, 12 lines, and 72 samples for the winter predictor and predictand sets, its associated "test" dataset contained 115 time points, 6 lines, and 18 samples. Then, separately for both the summer and winter test data, the time and space order of the data were each randomly permuted 100 times. For each of the 100 cases, the SVD decomposition was performed, and the mode N eigenvalues for all 100 cases were sorted in descending order, where $N = 1, \ldots, 10$. Thus, the first value in each sorted list gives the largest eigenvalue for the associated mode out of 100 randomly permuted datasets. For example, the first value in the mode-1 list gives the largest mode-1 eigenvalue of the 100 SVD procedures, the second value in that same list

gives the second largest mode-1 eigenvalue, and so forth. Similarly, the first value in the mode-2 list gives the largest mode-2 eigenvalue of the 100 SVD procedures, the second value in that same list gives the second largest mode 2 eigenvalue, and so forth. Thus, taking the first value in each list provides a Monte Carlo estimate of the 99% confidence limit for the eigenvalues found from the SVDs performed on the observed data. In this study, we chose those eigenmodes that had eigenvalues larger than this 99% significance level for all lead times for both seasons, in this case only the first three modes (cf. Preisendorfer et al. 1981; Overland and Preisendorfer 1982).

The predictions starting from the current pentad, Pentad0, with lead M pentads, are produced by taking the projection of the Pentad0 $-$ 1 and Pentad0 pentads onto the predictor patterns of the first three modes for the given lead time (e.g., upper panels of Figs. 4, 5, and 6 contain the predictor patterns for modes 1, 2, and 3 for an $M = 3$ pentad lead). This gives a projection coefficient for each of the three modes. Each projection co-

Mode 3 Winter Predictor

Mode 3 Summer Predictor

OLR (Wm^{-2})

Mode 3 Winter Predictand

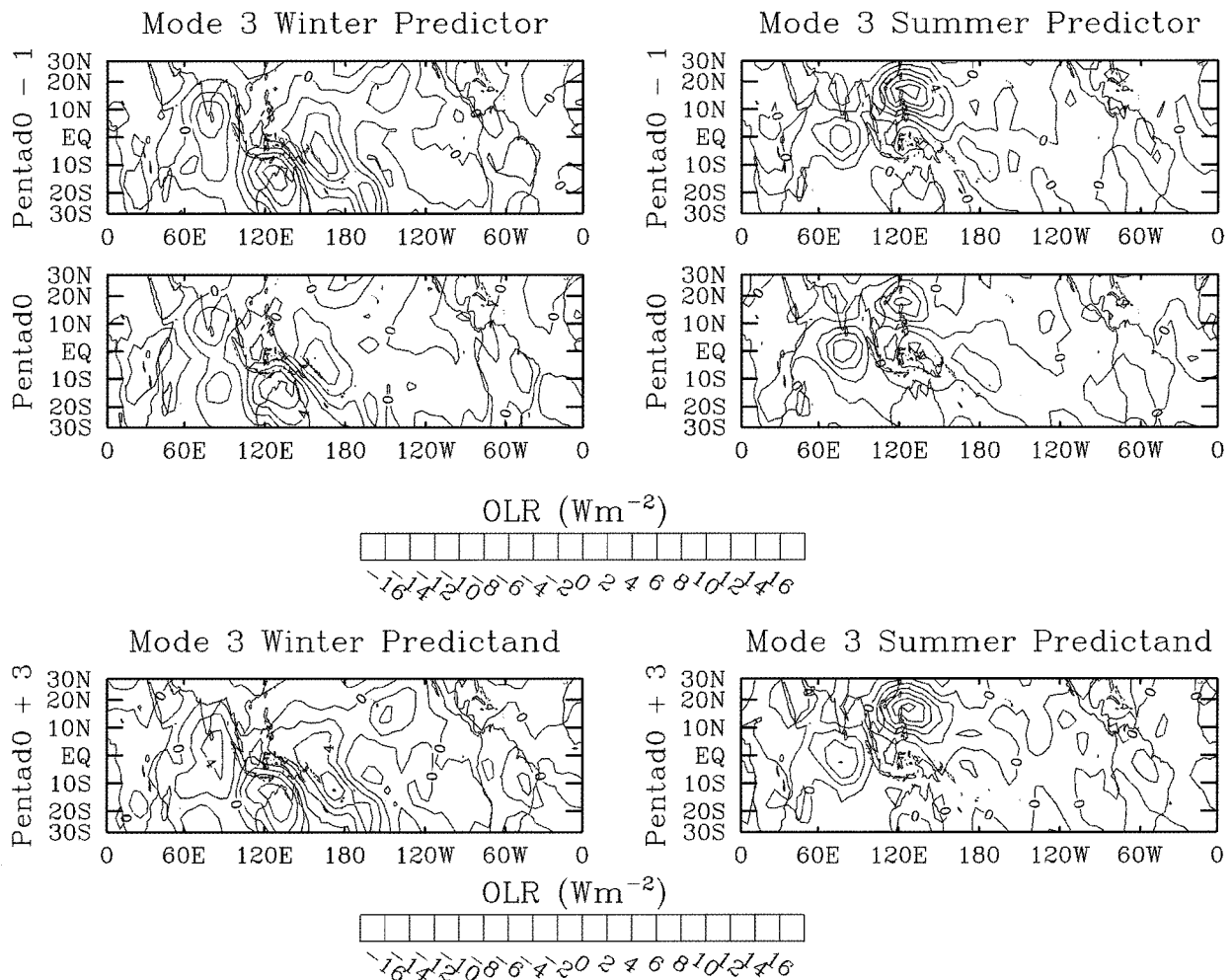## Mode 3 Summer Predictand

OLR (Wm^{-2})

FIG. 6. Same as Fig. 4, except for mode 3 for both Northern Hemisphere winter (left) and summer (right).

efficient is then multiplied by its associated predictand patterns (e.g., lower panels of Figs. 4, 5, and 6 contain the predictand patterns for modes 1, 2, and 3 for an $M = 3$ pentad lead), and then these weighted predictand patterns are summed together, giving an estimate of the bandpassed OLR anomalies at Pentad0 $+ M$ (cf. Graham et al. 1987).

3. Model validation and skill

The prediction scheme described in the previous section was cross-validated on the OLR data that was not used in the model development, that is, 1990–96. Figure 8 shows an example 3-pentad lead forecast, along with the corresponding validation data, in the form of a time–latitude diagram for summer 1992. The longitude range represented here is 75°–90°E. The observed anomalies (annual cycle removed) are in the upper panel, the band-passed anomalies are in the middle panel, and the forecast anomalies (which are inherently bandpassed) are in the lower panel. The validation data illustrate the slow

timescale of the MJO and show its impact on the onset and break periods of the summer Asian monsoon throughout the Indian Ocean and Indian subcontinent (e.g., Yasunari 1979; Lau and Chan 1988). The model forecast shows very good agreement with the bandpassed observations, which in turn have a fair resemblence to the total OLR anomalies. Of the three panels shown, the panel with the predicted OLR exhibits the smoothest variations in both time and space. This is due to the fact that the forecast model is based on data that have undergone both temporal bandpassing and modal filtering. The modes that are retained (i.e., leading three modes; see section 2 and Fig. 7) account for about 65%–70% of the covariance between the filtered predictor and predictand fields and about 27% of the variance of the filtered predictand field. To help assess the meteorology associated with the low-frequency fluctuations shown in Fig. 8, it is useful to note that in the Eastern Hemisphere warm pool areas, a 10 W m^{-2} OLR anomaly is approximately equal to a 2.0 mm day^{-1} rainfall anomaly (Xie and Arkin 1997). Therefore, the intraseasonal fluc-
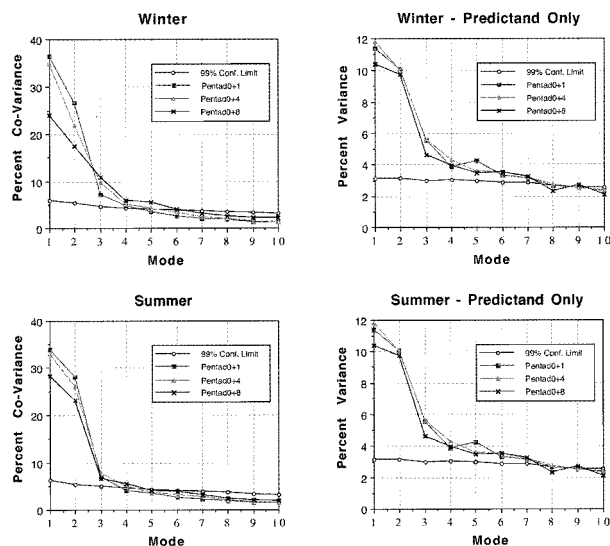
FIG. 7. (left panels) Percent covariance explained by the first 10 modes of the SVD decompositions for (top) winter and (bottom) summer models with lead times from 1, 4, and 8 pentads (box, triangle, and cross, respectively). (right panels) Same, except for percent variance explained by the predictands of the first 10 modes. In each case, estimates of 99% confidence limit is also shown (open dots).

tuations in rainfall induced by the MJO during this period are on the order of ± 0.5 cm day^{-1}. While the overall agreement is qualitatively good between the model and the observations, the time period between mid-July and mid-August illustrates an instance where the model's performance appears particularly poor. During this period the observations show an extended "wet" (negative OLR anomalies) period, encompassing about 40 days, north of the equator. For this same period, the model predicts the initial stage of the wet period fairly well; however, due to the intrinsic timescale associated with the model, it predicts a "dry" period to follow in early August, which is inconsistent with observed conditions.

Figure 9 shows a forecast similar to Fig. 8, except for 1992 winter conditions and a longitude range of 120°–135°E. In this case, the forecast and the associated validation data illustrate the intraseasonal influence of the MJO on the summer Australian monsoon (e.g., Hendon and Liebmann 1990a,b). Again, the model shows very good agreement with the bandpassed observations, which in turn show a fair resemblence to the total OLR anomalies. The agreement between the model and observations is best during January and February when a series of two strong MJO events propagate into the region and appear to produce a significant impact on northern Australian rainfall (~ 3 cm pentad^{-1} based on the scaling given above). These events are the same events that were captured by the Tropical Ocean Global Atmosphere Coupled Ocean–Atmosphere Response Experiment (COARE; Webster and Lucas 1992), and that

have been analyzed in a number of studies (e.g., Nakazawa 1995; Weller and Anderson 1996; Waliser et al. 1996; Lin and Johnson 1996; Lau and Sui 1997).

Figure 10 shows the above forecast in the form of a time–longitude diagram. In this case the latitude range extends from 10°S to 10°N. Again, the validating data in both bandpassed (middle panel) and total anomaly (left panel) forms are given. The extra lines at 150°E extending from the beginning of the forecast period through February indicate the overlapping COARE intensive observation period (IOP) at the site of the central Improved Meteorlogical (IMET) ocean/surface flux mooring (Weller and Anderson 1996). This set of observation data and forecasts for the COARE period is meant to illustrate the potential utility that might have been garnered from statistical forecasts of this kind during the IOP. For the strong intraseasonal events occurring during the IOP, that is, the two wet periods around 17 December and 20 January and the two dry periods around 10 January and 10 February, the statistical model appears to show some capability in providing advance (~ 15 days) notice of their arrival. Also evident during this period is a slow positive trend in total OLR anomaly, especially in the central and eastern Pacific, which is associated with large-scale, low-frequency ENSO variability. In the model's present design there has been no effort to incorporate the slowly varying component of the anomalies into the forecast. This aspect of the model and its possible improvements will be discussed in section 4. For the forecasts discussed above, the statistical model appears to show useful forecast skill over the Indian and western Pacific Oceans, and nearby land masses, out to at least 15 days. A more robust measure of the skill will be given below, which shows that the same level of model-data agreement can often extend out to 20-day lead times.

Figure 11 provides a global assessment of the model's predictive skill by illustrating the (temporal) correlation scores at each location and for lead times from 1 to 5 pentads against bandpassed observations. Winter (summer) correlation values are given in the left (right) panels. Note that the number of pentads incorporated in these plots is 263 for summer and 277 for winter. Autocorrelation values suggest that these sample sizes should be divided by about 6 to give a more realistic value for the number of independent samples. Therefore, being given about 40 independent samples for these computations implies a 99% confidence level on correlation values of 0.4. Model skill scores are highest in the Eastern Hemisphere where the MJO-related OLR variability is highest and where the dominant modes used in the model exhibit some predictive structure (i.e., Figs. 4–6). High values are between 0.7 and 0.9 and occur in some areas of the Indian Ocean, the Maritime Continent, and the western Pacific Ocean. Over much of the Eastern Hemisphere, the correlation values are about 0.5 for lead times extending out to 3 to 4 pentads. There are a few areas of high correlation over Africa
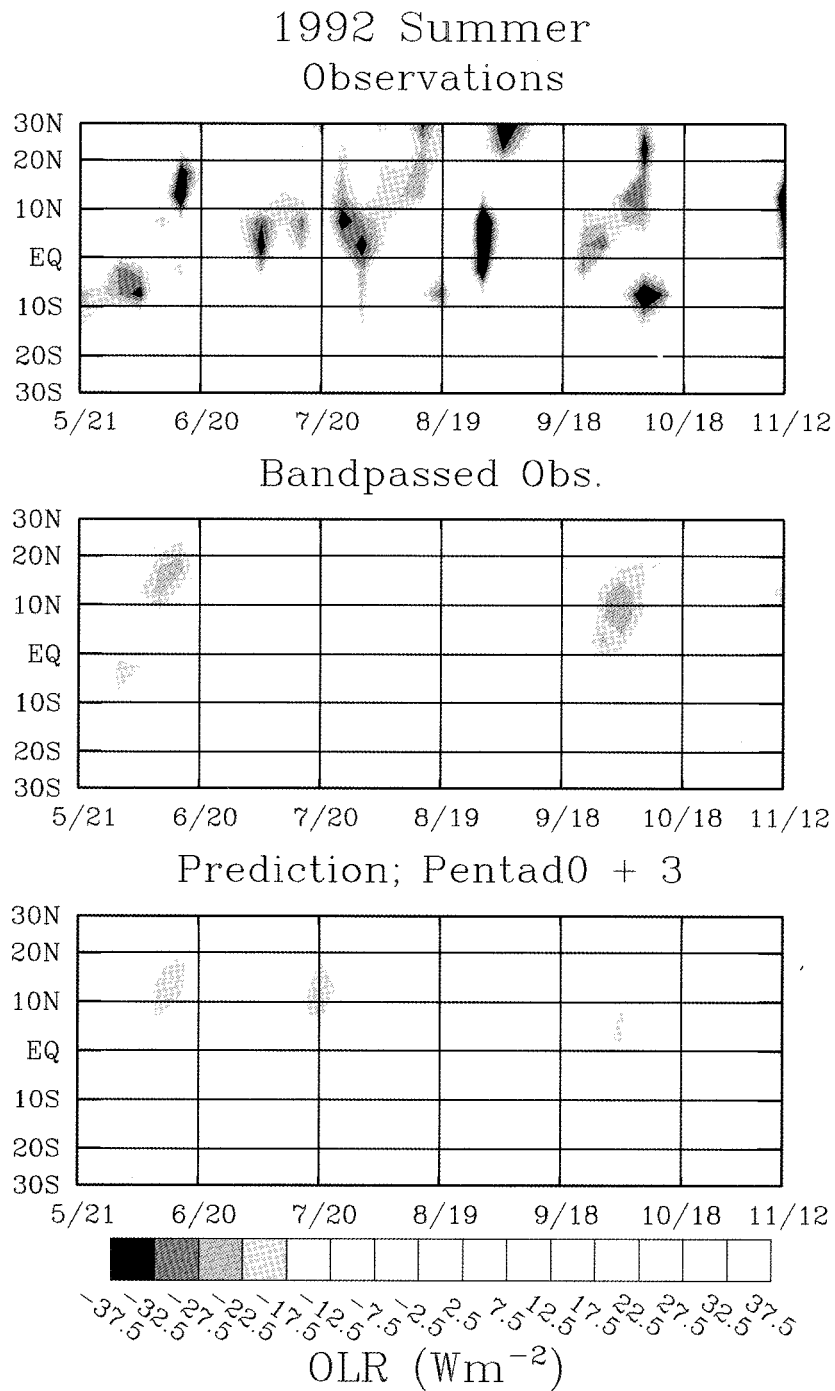
1992 Summer

Observations

Bandpassed Obs.

Prediction; Pentad0 + 3

OLR (Wm^{-2})

FIG. 8. Time–latitude plots of 3-pentad OLR prediction (lower; Pentad0 + 3), along with validating total (upper) and bandpassed (middle) OLR anomalies, for 1992 Northern Hemisphere summer. Data are averaged between 75° and 90°E.

and some modestly high values over portions of the tropical Americas. In addition to the higher correlation values found in both seasons in the equatorial warm-pool regions, the highest values for winter are biased toward northern Australia and the SPCZ, while those for summer are biased toward southeast Asia and the Indian subcontinent. In areas where the model seems to do well, the correlation values tend to remain high out to about 15 to 20 days, at which point they appear to diminish fairly rapidly.
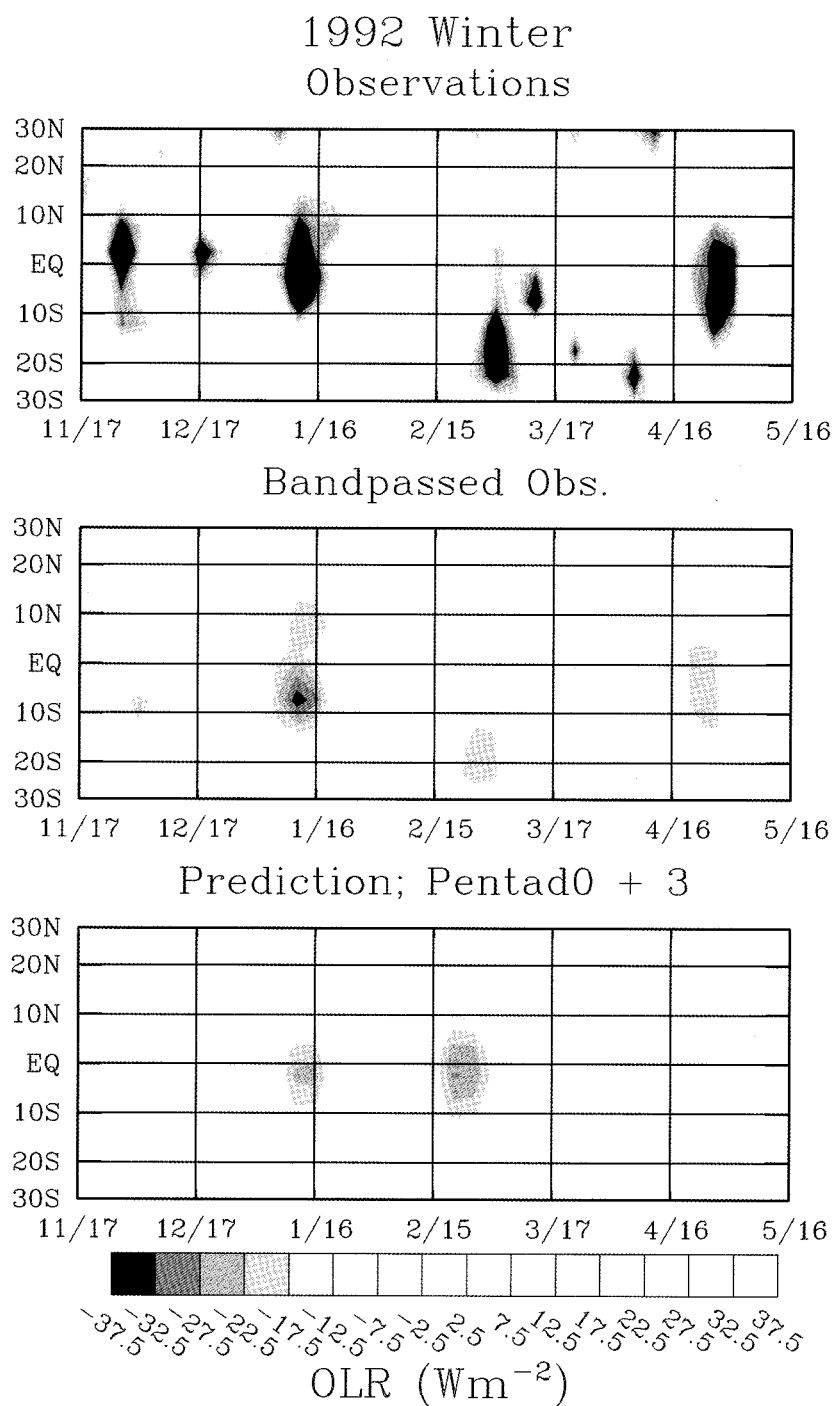
1992 Winter
Observations

Bandpassed Obs.

Prediction; Pentad0 + 3

OLR (Wm^{-2})

FIG. 9. Same as Fig. 8, except for 1992 Northern Hemisphere winter. Data are averaged between 120° and 135°E.

An estimate of the absolute errors associated with the statistical forecasts is provided in Fig. 12, which is similar to Fig. 11, except that it shows root-mean-square (rms) errors between the forecasts and the bandpassed data. Also, the lead times shown are for 1, 2, 3, 5, and 7 pentads to illustrate the size of the error at very long lead times. As with the correlation plots in Fig. 11, the rms errors remain relatively constant out to about 3 pentads, with further increases in lead time resulting in marked increases in the rms error. At short lead times, typical errors over a broad area of the Eastern Hemisphere are about 7–11 W m^{-2}, with errors in the deep
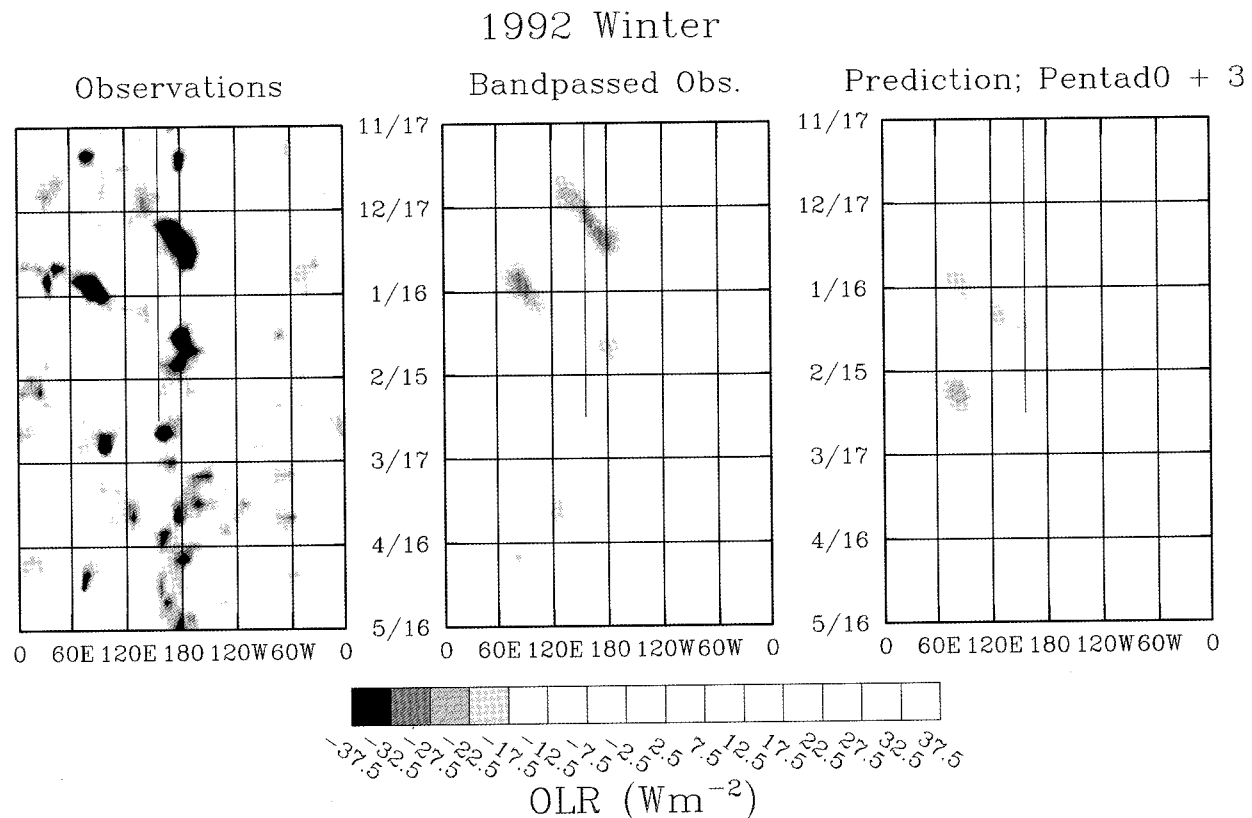
1992 Winter

FIG. 10. Time–longitude plots of 3-pentad OLR prediction (right; Pentad0 + 3), along with validating total (left) and bandpassed (center) OLR anomalies, for 1992 Northern Hemisphere winter. Data are averaged between 10°S and 10°N. Negative OLR values are shaded and indicate positive rainfall anomalies. Lines at 150°E extending from the beginning of the period through February indicate the overlapping COARE IOP at the site of the central IMET ocean/surface flux mooring.

Tropics reaching about 11–14 W m^{-2}. At very long leads, the errors increase to 14–18 W m^{-2}, and in fact the error structure at leads of 7 pentads is nearly the same, in both magnitude and structure, as the standard deviations of the bandpassed observations shown in Fig. 13. This is to be expected since there appears to be little or no forecast skill at these very long lead times, and thus the errors should be about the same size as the standard deviation of the observations.

A more conservative and practical measure of the model's skill is via comparisons to total anomaly data. Figure 14 shows a temporal correlation maps between model forecasts and total anomaly data for lead times from 1 to 5 pentads. The spatial structure is nearly identical to the structure of the correlation values against bandpassed data (Fig. 11), although the magnitude is considerably lower. Highest values in this case are about 0.4 to 0.5, with overall Eastern Hemisphere skill at lead times from about 1 to 4 pentads being more typically characterized by a correlation of 0.3. In the case of total anomalies, autocorrelation values suggest that the sample sizes (263 for summer and 277 for winter) should be divided by about 2–3 to give a realistic value for the number of independent samples. With 90 independent

samples, a correlation value of 0.3 is 99% significant. The reduction in model skill between the scores shown in Fig. 11 and those shown in Fig. 14 stems from the fact that the model only predicts variability between 30 and 70 days and thus is not providing an estimate of timescales outside this band (e.g., the low-frequency variability observed in the left panel of Fig. 10). Thus, these skill scores may be an underestimate of what a statistical model could do if a simplified method were incorporated to account for the low-frequency component over short lead times. For example, at lead times of 5–20 days, persistence might be a reasonable model to use for the low-frequency variability ($>$70 days, e.g., ENSO), which would improve the overall skill of the above type of model when compared to total anomaly data. On the other hand, the skill scores in both Figs. 11 and 14 are likely to be overestimates of the present model's skill in a true operational context due to the difficulty of producing a bandpassed estimate of the most recent 2 pentads. This aspect will be discussed in more detail in section 4.

To more easily see the degradation of the skill scores over time, Fig. 15 shows (temporal) correlation scores at a number of selected tropical cities/regions for both
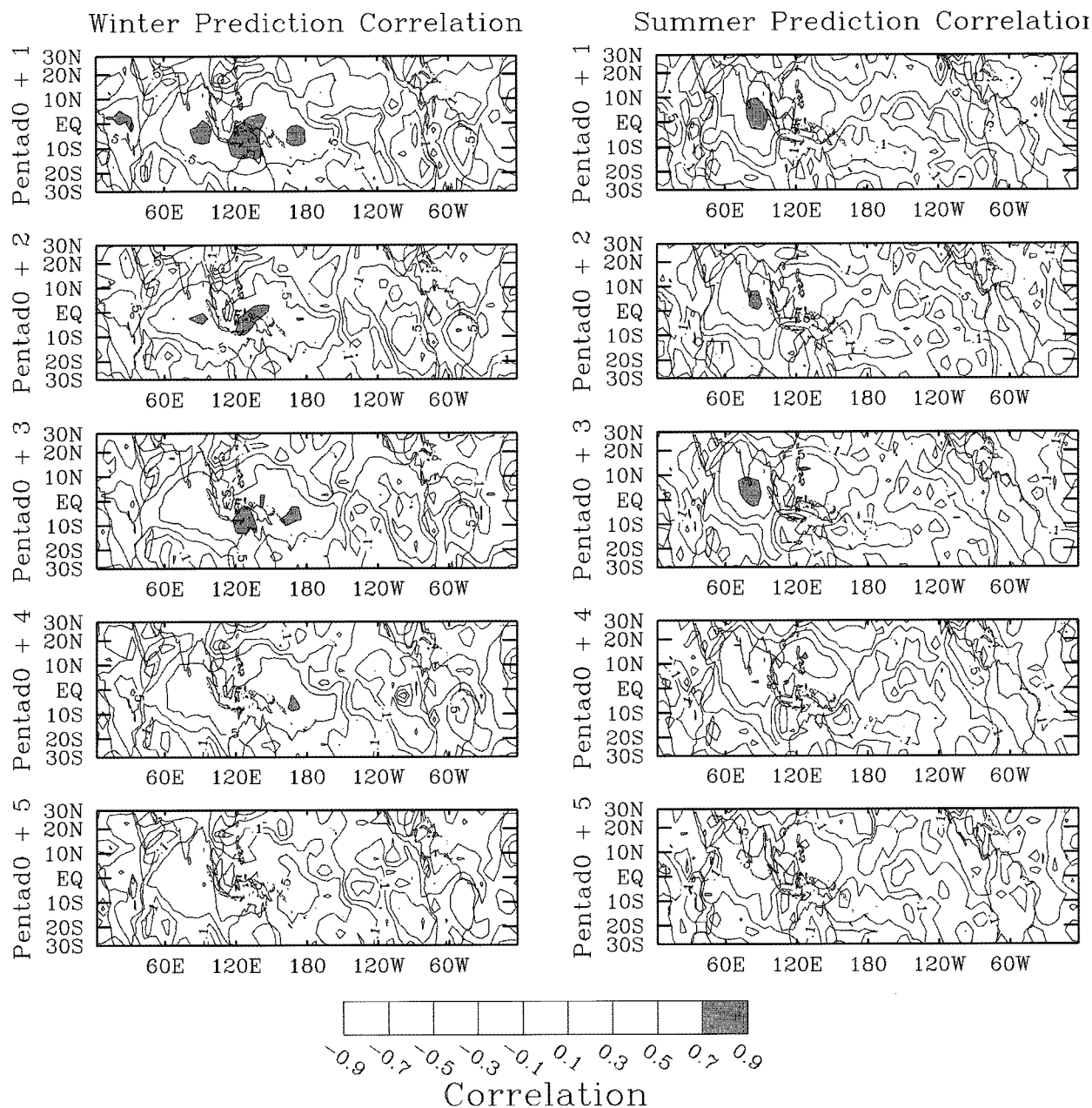
FIG. 11. Temporal correlations between predicted OLR and corresponding bandpassed observations for winter (left) and summer (right) seasons. Correlations are shown for lead times from 1 to 5 pentads, represented here as Pentad0 + 1, Pentad0 + 2, etc.

winter (top) and summer (bottom) plotted out to lead times of 9 pentads. The left panels show the skill scores against bandpassed data, and the right panels show the skill scores against total anomaly data. With the correlations plotted in this fashion, it is more evident that the model's skill is generally retained out to about 4 pentads, at which point it diminishes rapidly. Note that in a number of locations, the skill scores seem to diminish at 2 pentads, then rebound slightly at 3 and 4 pentads. The model appears to be most effective for

Darwin, Australia, and Nauru during the winter season, and Bombay, India; Maldives; Manila, Phillipines; and Columbo, Sri Lanka, in the summer season. Comparing the correlation values and the characteristic predictive timescales between these plots and those based on the NCEP MRF model (Figs. 1 and 2) illustrate that the statistical model appears to be significantly more skillful at predicting intraseasonal variability than the numerical forecast model analyzed here. These results suggest that a statistical model of the type presented here might pro-
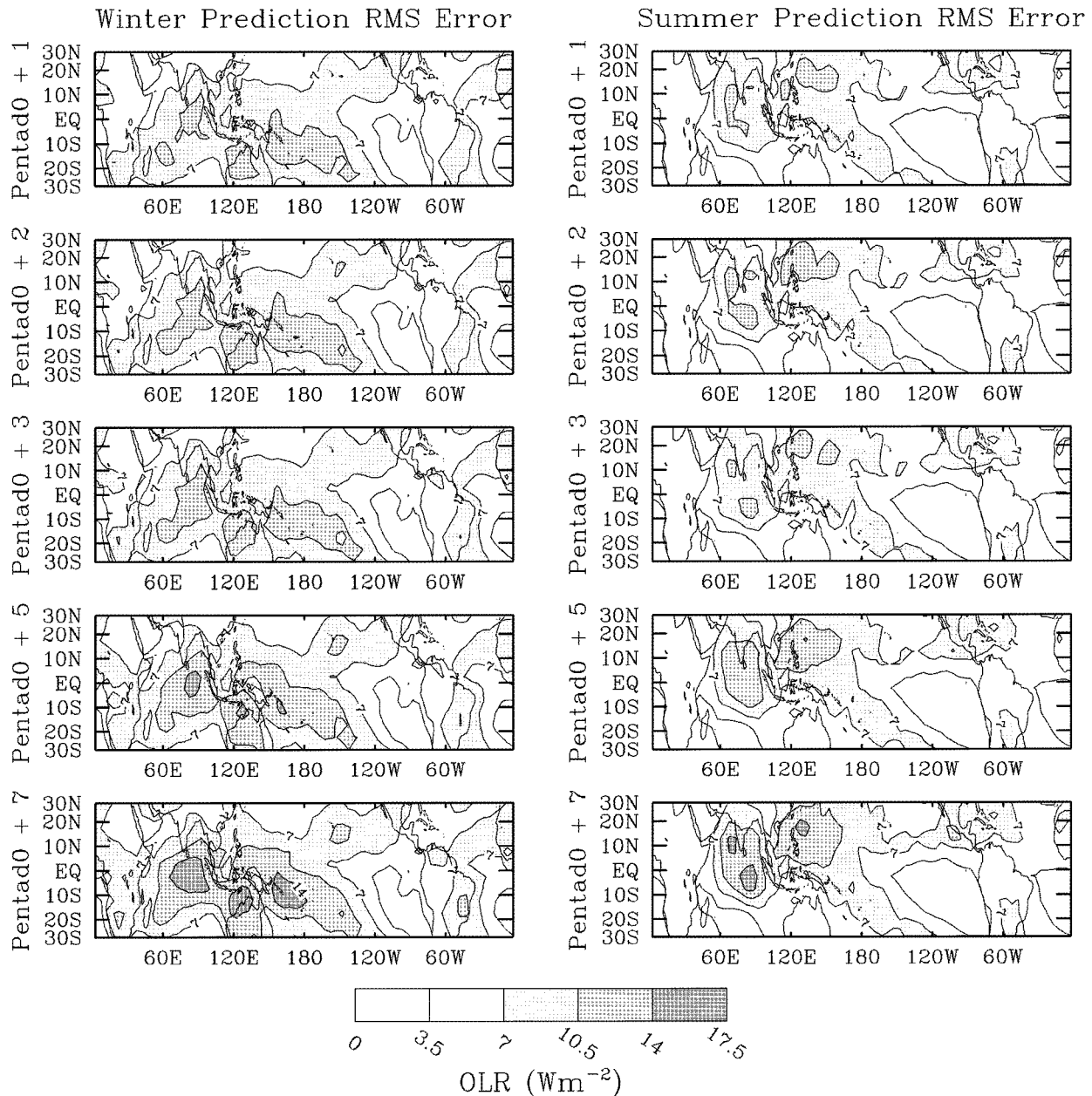
FIG. 12. Same as Fig. 11, except shows rms errors between predicted and OLR and corresponding bandpassed observations. Rms errors are shown for lead times of 1, 2, 3, 5, and 7 pentads.

vide an avenue for implementing improved extended-range operational forecasts in the Tropics. Furthermore, results such as these provide a benchmark by which to assess the predictive skill of extended-range tropical predictions from numerical forecast models.

4. Summary and discussion

In this study, we have presented the results from an analysis that explores the feasibility of using a statistical model to predict tropical rainfall variability at long lead times (i.e., 5–20 days). The statistical model is based on a field-to-field approach (i.e., SVD) which uses previous and present pentads of OLR, the predictors, to predict future pentads of OLR, the predictands (Figs. 4–6). The model was developed using 30–70-day bandpassed OLR data from 1979 to 1989 and validated on data from 1990 to 1996. For the validation period, the model exhibits temporal correlations to observed bandpassed data of about 0.5–0.9 over a significant region of the Eastern Hemisphere at lead times from 1 to 4 pentads, after which the correlation decreases signifi-
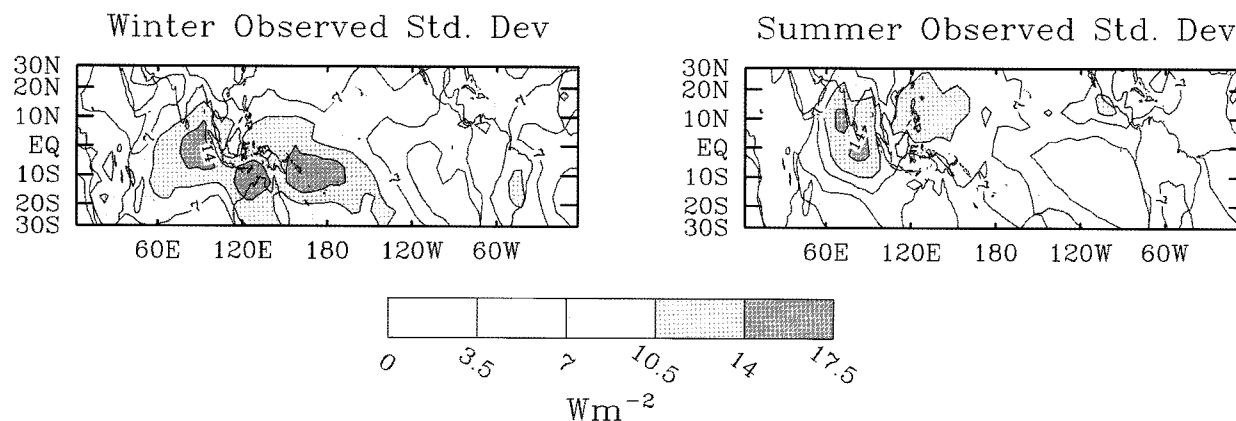
FIG. 13. Standard deviation of bandpassed anomalies from the validation period for winter (left) and summer (right).

cantly with increasing lead time (Figs. 11 and 15). Correlations against observed total anomalies are on the order of 0.3–0.5 over a smaller region of the Eastern Hemisphere (Fig. 14). Typical rms errors between model forecasts and the observed bandpassed data are between about 10–14 W m^{-2} out to lead times of 3 to 4 pentads (Fig. 12; cf. Fig. 13).

Before arriving at the OLR-based model presented in this article, several variations were tested to determine an ''optimal'' configuration. For example, models based on predictors having only 1 pentad were not as skillful as the model described above with predictors having 2 pentads. Predictors made up of 3 pentads showed a very slight improvement at 5–10-day leads but a very slight degradation at longer leads. In addition, the predictor fields were also augmented with dynamic fields from the NCEP–National Center for Atmospheric Research (NCAR) reanalysis (Kalnay et al. 1996) to determine if the addition of this type of information would improve the model's skill. Tests were done with predictor fields made up of OLR plus 200-mb zonal wind, OLR plus 850-mb zonal wind, and OLR plus 200-mb velocity potential. None of these combined predictor fields showed any noticeable improvement in the model skill over those containing OLR alone. It should be noted, however, that at the time these tests with additional data were done, the bandpassed data included periods from 20 to 100 days instead of the 30–70 days presented here. While we suspect that the reduced bandwidth of the filter would not change this conclusion, the dynamic augmentation of the predictors with more optimal configurations might still warrant further investigation. It is also worth mentioning that the forecast model was originally developed for just the Eastern Hemisphere since it was expected to have the most skill there. Extending the model domain to the global Tropics did not show any appreciable improvement/degradation in skill for the Eastern Hemisphere, but since the full tropical model showed some skill at short lead times in and around Central/South America, it was left in for completeness' sake. Finally, canonical correlation analysis was applied instead of SVD with nearly identical results.

Our motivation for undertaking this modeling effort was based on addressing two objectives. The first objective was to provide an initial assessment of how well a statistical model might perform in forecasting rainfall variability, which is modulated by the MJO. This objective was one of the main reasons the model development was based on OLR anomalies. The second objective stemmed from our interest in assessing the predictive skill of the dynamical extended range forecasts (DERFs) from the NCEP MRF model (Schemm et al. 1996). Based on the figures of the DERF 200-mb zonal velocity skill shown in the introduction (Figs. 1 and 2) and those for the OLR-based statistical model, it would appear that at present statistical models may have the advantage over the current version of the NCEP MRF model. To make a more direct comparison between the statistical and dynamical models, we also constructed a statistical model using the same methodology outlined for the OLR-based model (section 2), except that in this case we used 200-mb zonal winds as the predictors and predictands. Pentad average zonal winds were obtained from the NCEP–NCAR reanalysis product (Kalnay et al. 1996). Model development was based on the 11-yr period from 1976 to 1986. In this case, the percentage of covariance accounted for by the first three modes retained for the model was about 72% and the percentage of variance in the predictands was about 31%. Further, the principal modes for the zonal wind model had similar levels of confidence as those for the OLR model (Fig. 7).

Validation of the 200-mb zonal wind model was performed on the subsequent 7 yr of data, from 1987 to 1993. Figure 16 shows the temporal correlations between the predicted and observed bandpassed data for lead times between 1 and 5 pentads. In contrast to the associated figure for the OLR-based model (Fig. 11),
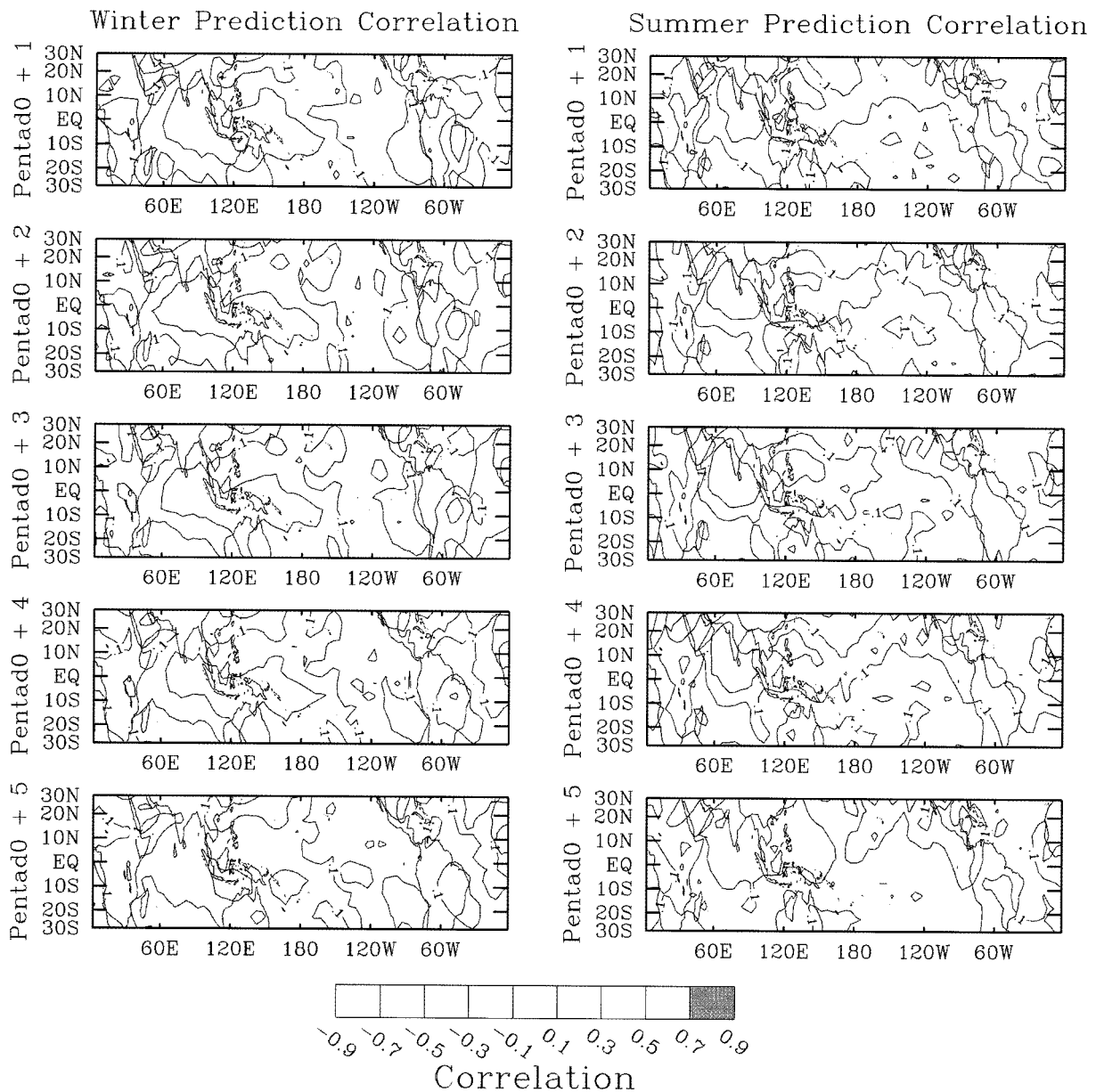
FIG. 14. Same as Fig. 11, except shows correlations between predicted OLR and corresponding total OLR anomalies.

the correlations are more zonally uniform throughout the Tropics (which is also the case for the spatial structure of the principal SVD modes, not shown). While the maximum correlation values at any given lead time for the zonal wind model are about the same as those for the OLR model, they tend to cover a much larger area at each lead time leading to a better model–data agreement overall. Figure 17 shows an example of a specific prediction for the bandpassed 200-mb zonal winds for winter of 1987 in the form of an equatorial time–longitude plot. The results in these last two figures are presented for comparison to the results shown in Figs.

1 and 2, which indicated that useful predictive skill for the DERF extends out to only about 5–10 days. For the statistical model, however, it is readily apparent that considerable similarity exists between the model and the observations out to at least 10 days and even to a large extent out to 20 days. These results indicate that considerable advantage might be afforded from the further exploration and eventual implementation of the above types of statistical models to augment current operational long-range forecasts in the Tropics. Moreover, they also indicate that there is considerably more work to be done in achieving the likely forecast potential

Compared to Bandpassed Data
Model Prediction Skill - Winter

Compared to Anomaly Data
Model Prediction Skill - Winter

Model Prediction Skill - Summer
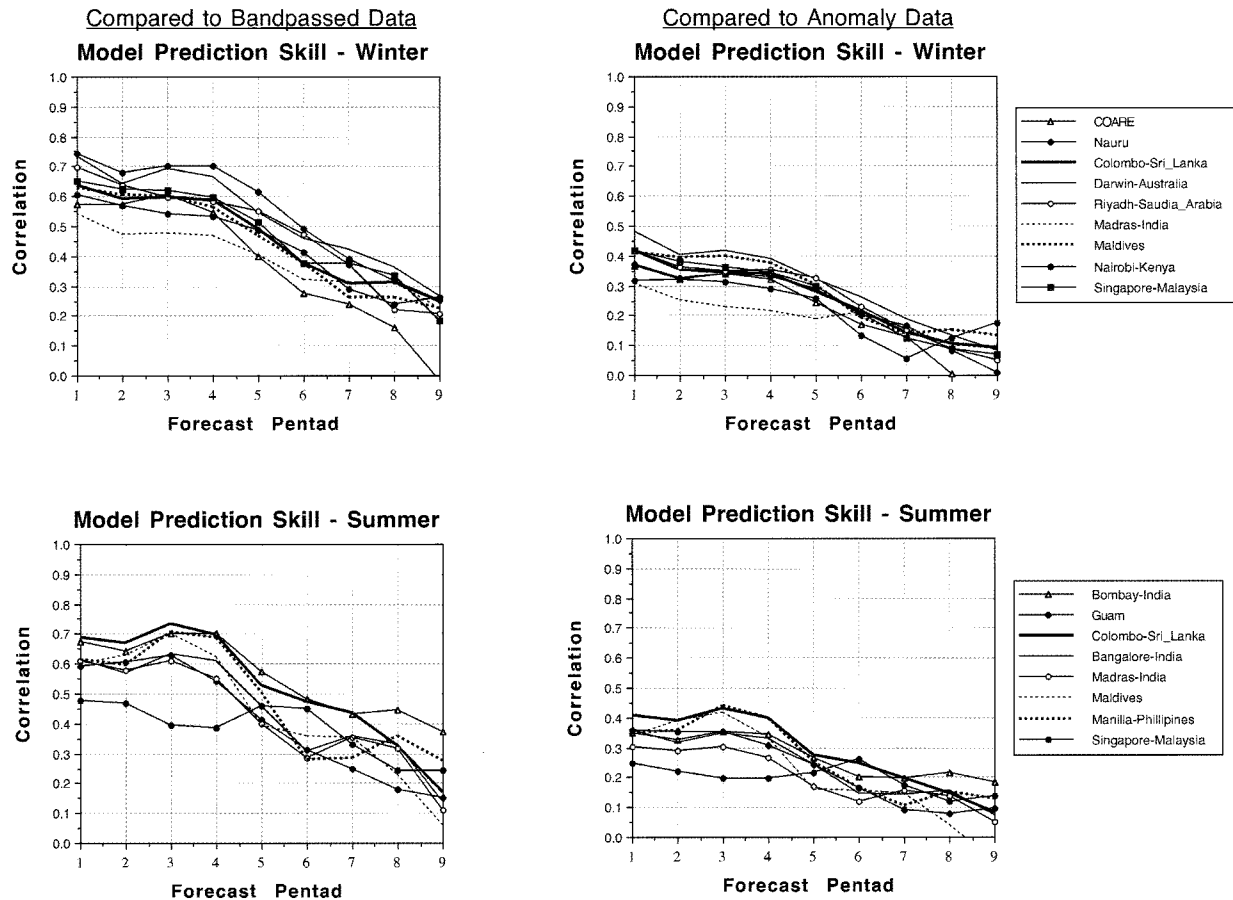
Model Prediction Skill - Summer

FIG. 15. Temporal correlations between predicted OLR and validating observations for Northern Hemisphere winter (top) and summer (bottom) based on comparisons to bandpassed data (left) and total anomaly (annual cycle removed) data (right) at a number of cities in the Tropics.

that dynamic models might offer if they could suitably simulate MJO variability. We are presently analyzing the DERF predictive skill in more detail to better understand the variability of the MJO in the NCEP MRF model (Jones et al. 1999, manuscript submitted to *Climate Dyn.*; cf. Hendon et al. 1999) and to help improve the physical parameterizations that help to maintain its temporal and spatial structure.

The relatively high skill values illustrated by the statistical models out to lead times of 3 to 4 pentads offers some hope that such a model might be a useful tool in an operational context. The main hurdle in generating operational predictions from the present scheme is producing an accurate bandpassed estimate of the 2 most recent pentads (i.e., the predictor). These pentads essentially are endpoints of time series and conventional/typical bandpass methods can produce spurious endpoint behavior. Performing tests on a sequence of two years' worth of sample pentad data shows that the bandpassed predictor patterns resulting from a record extending well beyond the endpoint (in a hindcast sense)

and those resulting from endpoint conditions typically correlate in space at about 0.9 using the 29-point Lanczos filter applied here. A shorter filter would improve this a bit but would lead to a diminished overall frequency response by reducing its peak amplitude and broadening its width. Fortunately, it was found that the more energy that the predictor has in the principal two modes, the more likely the correlation is above 0.9, and vice versa. Thus when there is a strong MJO component in the weather/climate system, the bandpassed predictor is less likely to contain spurious signals. However, even a factor of 0.9 would reduce the skill scores a sizable fraction, given that the predictor pattern would only encapsulate about 81% of the "real" bandpassed variance.

Efforts are under way to improve the model with respect to this operational consideration. A number of alternatives need to be investigated. One would be to try an iterative approach by which data from the first prediction is used to pad the end of the original anomaly record, upon which a second bandpassed estimate could
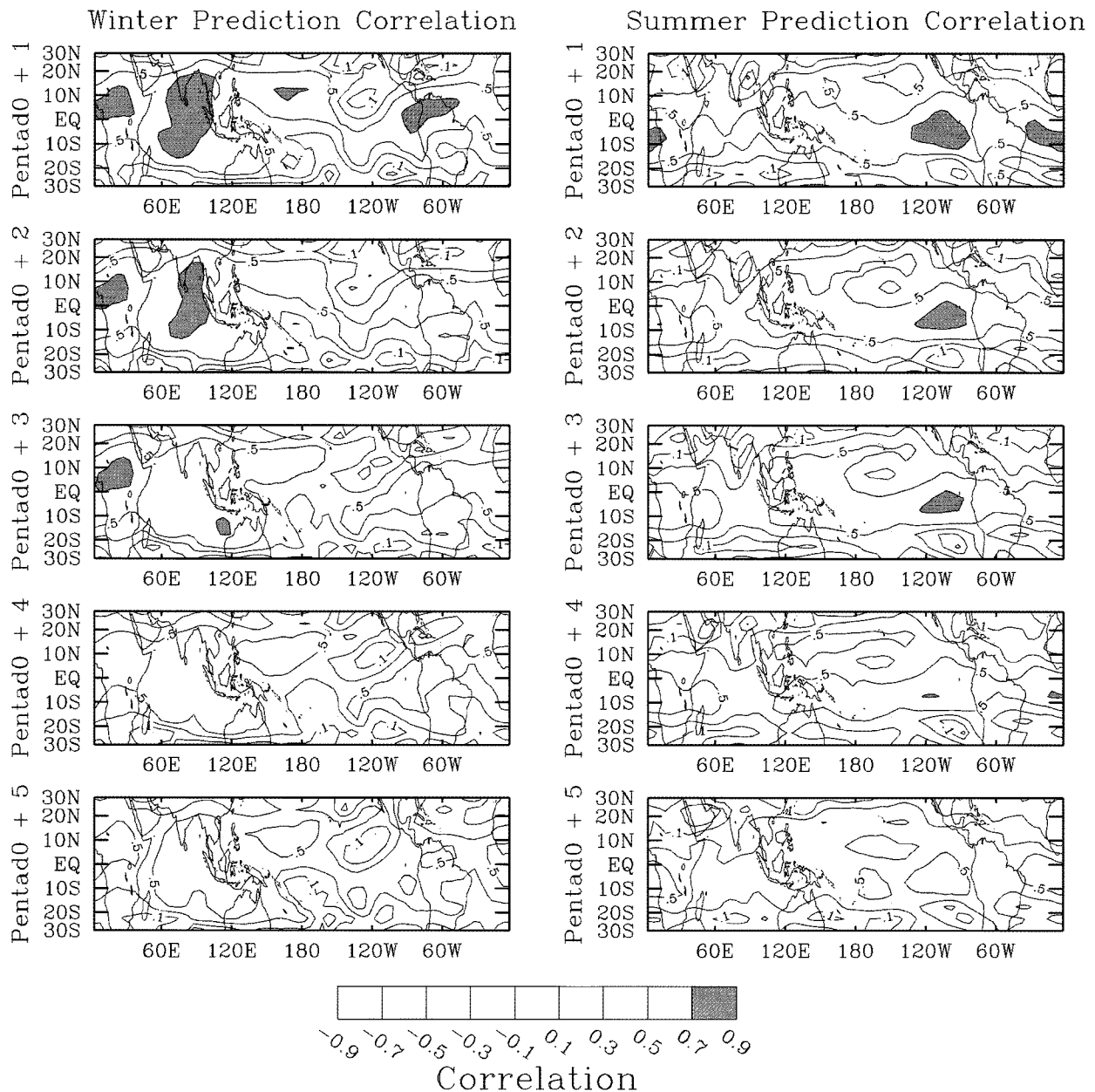
FIG. 16. Same as Fig. 11, except for a statistical model based on 200-mb zonal winds as both predictor and predictand.

be made. This might require making some estimate of the low-frequency trends as well since any dramatic change in the low-frequency components between the actual end of the record, and that component that has been artificially padded onto the end would likely result in the generation of artificial high-frequency signals, which would contaminate the intraseasonal band. Regardless of the approach taken to solve the bandpassed endpoint problem, having a method to forecast the low-frequency component (e.g., persistence) will be a useful addition for a model such as that discussed here when

it is put into operational use. Other alternatives for solving the above problem might be to use separate techniques for removing the high and low frequencies. Low-frequency signal (i.e., ENSO variability) might be removed using low-order empirical orthogonal functions, and high-frequency signals could be removed by using longer time averages that could even overlap to retain some aspect of the high temporal resolution (e.g., overlapping 10-day averages every 5 days). If an effective method could be developed to remove the low-frequency component, then the additional filtering needed
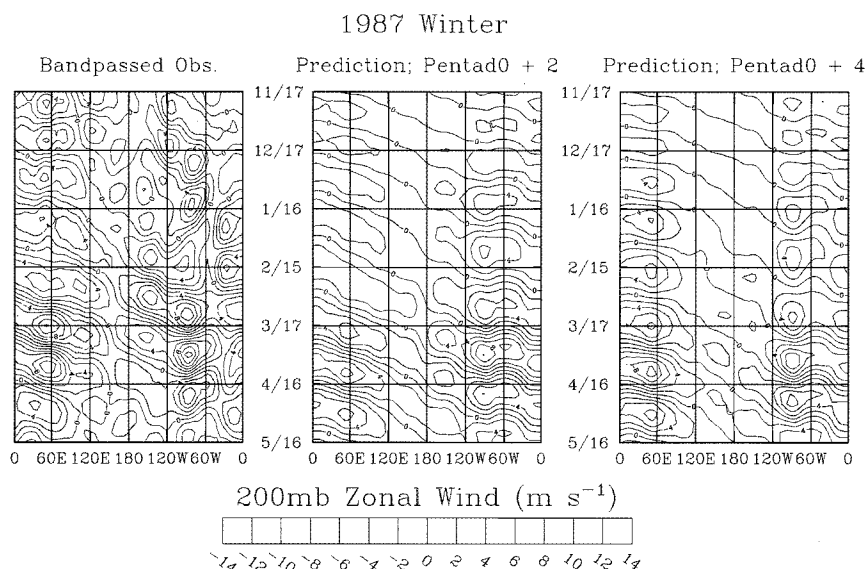
1987 Winter

FIG. 17. Time–longitude plots of Pentad0 + 2 and Pentad0 + 4 bandpassed 200-mb zonal wind predictions (middle and right, respectively), along with validating bandpassed anomalies (left), for 1987 Northern Hemisphere winter. Data are averaged between 10°S and 10°N.

to remove high frequencies/wavenumbers could be done in space rather than time, since most of the intraseasonal energy is contained within wavenumbers 1–3 (Salby and Hendon 1994).

REFERENCES

Arkin, P. A., and P. E. Ardanuy, 1989: Estimating climatic-scale precipitation from space: A review. *J. Climate, 2,* 1229–1238.

Bretherton, C. S., C. Smith, and J. M. Wallace, 1992: An intercomparison of methods for finding coupled patterns in climate data. *J. Climate, 5,* 541–560.

Brooks, C. E. P., and N. Carruthers, 1953: *Handbook of Statistical Methods in Meteorology.* Her Majesty's Stationery Office, 412 pp.

Cane, M. A., S. E. Zebiak, and S. C. Dolan, 1986: Experimental forecasts of El Nino. *Nature, 321,* 827–832.

Chang, C. P., and H. Lim, 1988: Kelvin Wave-CISK: A possible mechanism for the 30–50 day oscillation. *J. Atmos. Sci., 45,* 1709–1720.

Chen, T.-C., and J. C. Alpert, 1990: Systematic errors in the annual and intraseasonal variations of the planetary-scale divergent circulation in NMC medium-range forecasts. *Mon. Wea. Rev., 118,* 2607–2623.

Duchon, C. E., 1979: Lanczos filter in one and two dimensions. *J. Appl. Meteor., 18,* 1016–1022.

Emanuel, K. A., 1987: An air–sea interaction model of intraseasonal oscillations in the Tropics. *J. Atmos. Sci., 44,* 2324–2340.

Ferranti, L., T. N. Palmer, F. Molteni, and K. Klinker, 1990: Tropical–extratropical interaction associated with the 30–60 day oscillation and its impact on medium and extended range prediction. *J. Atmos. Sci., 47,* 2177–2199.

Gill, A. E., and E. M. Rasmusson, 1983: The 1982–83 climate anomaly in the equatorial Pacific. *Nature, 305,* 229–234.

Graham, N. E., 1995: Simulation of recent global temperature trends. *Science, 267,* 666–671.

——, and T. P. Barnett, 1987: Sea surface temperature, surface wind divergence, and convection over tropical oceans. *Science, 238,* 657–659.

——, and ——, 1995: ENSOs and ENSO-related predictability. Part II: Northern Hemisphere 700-mb height predictions based on a hybrid coupled ENSO model. *J. Climate, 8,* 544–549.

——, J. Michaelsen, and T. P. Barnett, 1987: An investigation of the El Niño–Southern Oscillation cycle with statistical models. 1. Predictor field characteristics. *J. Geophys. Res., 92,* 14 251–14 270.

Gray, W. M., C. W. Landsea, P. W. Mielke Jr., and K. J. Berry, 1992: Predicting Atlantic seasonal hurricane activity 6–11 months in advance. *Wea. Forecasting, 7,* 440–455.

Gruber, A., and A. F. Krueger, 1984: The status of the NOAA outgoing longwave radiation dataset. *Bull. Amer. Meteor. Soc., 65,* 958–962.

Gutzler, D. S., and T. M. Wood, 1990: Structure of large-scale convection anomalies over tropical oceans. *J. Climate, 3,* 483–496.

Hayashi, Y. Y., and A. Sumi, 1986: The 30–40 day oscillations simulated in an "Aqua-Planet" model. *J. Meteor. Soc. Japan, 64,* 451–467.

Hendon, H. H., 1988: A simple model of the 40–50 day oscillation. *J. Atmos. Sci. 45,* 569–584.

——, and B. Liebmann, 1990a: A composite study of onset of the Australian summer monsoon. *J. Atmos. Sci., 47,* 2227–2240.

—, and —, 1990b: The intraseasonal (30–50 day) oscillation of the Australian summer monsoon. *J. Atmos. Sci.,* **47,** 2909–2923.

—, and M. L. Salby, 1994: The life cycle of the Madden and Julian Oscillation. *J. Atmos. Sci.,* **51,** 2225–2237.

—, and J. Glick, 1997: Intraseasonal air–sea interaction in the tropical Indian and Pacific Oceans. *J. Climate,* **10,** 647–661.

—, B. Liebmann, M. Newman, J. D. Glick, and J. E. Schemm, 1999: Medium-range forecast errors associated with active episodes of the Madden–Julian oscillation. *Mon. Wea. Rev.,* in press.

Higgins, R. W., and K. C. Mo, 1997: Persistent North Pacific circulation anomalies and the tropical intraseasonal oscillation. *J. Climate,* **10,** 223–244.

Janowiak, J. E., and P. A. Arkin, 1991: Rainfall variations in the Tropics during 1986–89, as estimated from observations of cloud-top temperature. *J. Geophys. Res.,* **96** (Suppl.), 3359–3373.

Ji, M., A. Kumar, and A. Leetma, 1994: A multi-season climate forecast system at the National Meteorological Center. *Bull. Amer. Meteor. Soc.,* **75,** 569–577.

Jones, C., D. E. Waliser, and C. Gautier, 1998: The influence of the Madden–Julian oscillation on ocean surface heat fluxes and sea surface temperature. *J. Climate,* **11,** 1057–1072.

Kalnay, E., and Coauthors, 1996: NCEP/NCAR 40-Year Reanalysis Project. *Bull. Amer. Meteor. Soc.,* **77,** 437–471.

Kanamitsu, M., 1985: A study of the predictability of the ECMWF operational forecast model in the tropics. *J. Meteor. Soc. Japan,* **63,** 779–804.

Kessler, W. S., M. J. McPhaden, and K. M. Weickmann, 1996: Forcing of intraseasonal Kelvin waves in the equatorial Pacific. *J. Geophys. Res.,* **100,** 10 613–10 631.

Knutson, T. R., and K. M. Weickmann, 1987: The 30–60 day atmospheric oscillation: Composite life cycles of convection and circulation anomalies. *Mon. Wea. Rev.,* **115,** 1407–1436.

Kousky, V. E., and M. T. Kayano, 1993: Real-time monitoring of intraseasonal oscillations. *Proc. 18th Annual Climate Diagnostics Workshop,* Boulder, CO, NCEP/NOAA, 66–69.

Landsea, C. W., W. M. Gray, P. W. Mielke Jr., and K. J. Berry, 1994: Seasonal forecasting of Atlantic hurricane activity. *Weather,* **49,** 273–284.

Lau, K. M., and P. H. Chan, 1985: Aspects of the 40–50 day oscillation during the northern winter as inferred from outgoing longwave radiation. *Mon. Wea. Rev.,* **113,** 1889–1909.

—, and —, 1986: Aspects of the 40–50 day oscillation during the northern summer as inferred from outgoing longwave radiation. *Mon. Wea. Rev.,* **114,** 1354–1367.

—, and T. J. Phillips, 1986: Coherent fluctuations of extratropical geopotential height and tropical convection in intraseasonal time scales. *J. Atmos. Sci.,* **43,** 1164–1181.

—, and L. Peng, 1987: Origin of low-frequency (intraseasonal) oscillations in the tropical atmosphere. Part I: Basic theory. *J. Atmos. Sci.,* **44,** 950–972.

—, and P. H. Chan, 1988: Intraseasonal and interannual variations of tropical convection: A possible link between the 40–50 day oscillation and ENSO? *J. Atmos. Sci.,* **45,** 506–521.

—, and F. C. Chang, 1992: Tropical intraseasonal oscillation and its prediction by the NMC operational model. *J. Climate,* **5,** 1365–1378.

—, and C. H. Sui, 1997: Mechanisms of short-term sea surface temperature regulation: Observations during TOGA COARE. *J. Climate,* **10,** 465–472.

Liebmann, B., and D. L. Hartmann, 1984: An observational study of tropical–midlatitude interaction on intraseasonal time scales during winter. *J. Atmos. Sci.,* **41,** 3333–3350.

Lin, X., and R. H. Johnson, 1996: Kinematic and thermodynamic characteristics of the flow over the western Pacific warm pool during TOGA COARE. *J. Atmos. Sci.,* **53,** 695–715.

Madden, R. A., and P. R. Julian, 1971: Detection of a 40–50 day oscillation in the zonal wind in the tropical Pacific. *J. Atmos. Sci.,* **28,** 702–708.

—, and —, 1994: Observations of the 40–50 day tropical oscillation: A review. *Mon. Wea. Rev.,* **122,** 814–837.

Mason, S. J., L. Goddard, N. E. Graham, E. Yulaeva, L. Sun, and P. Arkin, 1999: The IRI seasonal climate prediction system and the 1997/98 El Niño event. *Bull. Amer. Meteor. Soc.,* in press.

McPhaden, M. J., and B. A. Taft, 1988: Dynamics of seasonal and intraseasonal variability in the eastern equatorial Pacific. *J. Phys. Oceanogr.,* **18,** 1713–1732.

Morrissey, M. L., 1986: A statistical analysis of the relationships among rainfall, outgoing longwave radiation and the moisture budget during January–March 1979. *Mon. Wea. Rev.,* **114,** 931–942.

—, and N. E. Graham, 1996: Recent trends in rain gauge precipitation measurements from the tropical Pacific: Evidence for an enhanced hydrologic cycle. *Bull. Amer. Meteor. Soc.,* **77,** 1207–1219.

Murakami, T., 1979: Large-scale aspects of deep convective activity over the GATE area. *Mon. Wea. Rev.,* **107,** 994–1013.

Nakazawa, T., 1995: Intraseasonal oscillations during the TOGA-COARE IOP. *J. Meteor. Soc. Japan,* **73,** 305–319.

Neelin, J. D., I. M. Held, and K. H. Cook, 1987: Evaporation-wind feedback and low-frequency variability in the tropical atmosphere. *J. Atmos. Sci.,* **44,** 2341–2348.

Nitta, T., and S. Yamada, 1989: Recent warming of the tropical sea surface temperature and its relationship to the Northern Hemisphere circulation. *J. Meteor. Soc. Japan,* **67,** 375–383.

Overland, J. E., and R. W. Preisendorfer, 1982: A significance test for principal components applied to a cyclone climatology. *Mon. Wea. Rev.,* **110,** 1–4.

Preisendorfer, R. W., F. W. Zwiers, and T. P. Barnett, 1981: Foundations of principal component selection rules. SIO Rep. 81-7, Scripps Institution of Oceanography, 200 pp.

Rasmusson, E. M., and J. M. Wallace, 1983: Meteorological aspects of the El Niño/Southern Oscillation. *Science,* **222,** 1195–1202.

Reynolds, C. A., P. Webster, and E. Kalnay, 1994: Random error growth in NMC's global forecasts. *Mon. Wea. Rev.,* **122,** 1281–1305.

Salby, M. L., and H. H. Hendon, 1994: Intraseasonal behavior of clouds, temperature and motion in the Tropics. *J. Atmos. Sci.,* **51,** 2207–2224.

—, R. Garcia, and H. H. Hendon, 1994: Planetary circulations in the presence of climatological and wave-induced heating. *J. Atmos. Sci.,* **51,** 2344–2367.

Schemm, J. E., H. M. van den Dool, and S. Saha, 1996: A Multi-Year DERF Experiment at NCEP. Preprints, *11th Conf. on Numerical Weather Prediction,* Norfolk, VA, Amer. Meteor. Soc., 47–49.

Slingo, J. M., and Coauthors, 1996: Intraseasonal oscillations in 15 atmospheric general circulation models: Results from an AMIP diagnostic subproject. *Climate Dyn.,* **12,** 325–357.

van den Dool, H. M., 1994: Long-range weather forecasts through numerical and empirical methods. *Dyn. Atmos. Oceans,* **20,** 247–270.

—, and S. Saha, 1990: Frequency dependence in forecast skill. *Mon. Wea. Rev.,* **118,** 128–137.

von Storch, H., and J. Xu, 1990: Principal oscillation pattern analysis of the 30- to 60-day oscillation in the tropical troposphere. *Climate Dyn.,* **4,** 175–190.

Waliser, D. E., and N. E. Graham, 1993: Convective cloud systems and warm-pool SSTs: Coupled interactions and self-regulation. *J. Geophys. Res.,* **98** (D7), 12 881–12 893.

—, and W. Zhou, 1997: Removing satellite equatorial crossing time biases from the OLR and HRC datasets. *J. Climate,* **10,** 2125–2146.

—, N. E. Graham, and C. Gautier, 1993: Comparison of the highly reflective cloud and outgoing longwave datasets for use in estimating tropical deep convection. *J. Climate,* **6,** 331–353.

—, W. D. Collins, and S. P. Anderson, 1996: An Estimate of the surface shortwave cloud forcing over the western Pacific during TOGA COARE. *Geophys. Res. Lett.,* **23,** 519–522.

——, K. M. Lau, and J. H. Kim, 1999: The influence of coupled sea surface temperatures on the Madden–Julian oscillation: A model perturbation experiment. *J. Atmos. Sci.,* **56,** 333–358.

Wang, B., and H. Rui, 1990a: Dynamics of the coupled moist Kelvin–Rossby wave on an equatorial beta plane. *J. Atmos. Sci.,* **47,** 397–413.

——, and ——, 1990b: Synoptic climatology of transient tropical intraseasonal convection anomalies. *Meteor. Atmos. Phys.,* **44,** 43–61.

——, and X. Xie, 1998: Coupled modes of the warm pool climate system. Part I: The role of air–sea interaction in maintaining Madden–Julian oscillation. *J. Climate,* **11,** 2116–2135.

Webster, P. J., and R. Lucas, 1992: TOGA COARE: The Coupled Ocean–Atmosphere Response Experiment. *Bull. Amer. Meteor. Soc.,* **73,** 1377–1416.

Weickmann, K. M., 1983: Intraseasonal circulation and outgoing longwave radiation modes during Northern Hemisphere winter. *Mon. Wea. Rev.,* **111,** 1838–1858.

——, 1991: El Niño/Southern Oscillation and Madden–Julian (30–60 day) oscillations during 1981–1982. *J. Geophys. Res.,* **96,** 3187–3195.

——, G. R. Lussky, and J. E. Kutzbach, 1985: Intraseasonal (30–60 day) fluctuations of outgoing longwave radiation and 250-mb stream function during northern winter. *Mon. Wea. Rev.,* **113,** 941–961.

Weller, R. A., and S. A. Anderson, 1996: Temporal variability and mean values of the surface meteorology and air–sea fluxes in the western equatorial Pacific warm pool during TOGA COARE. *J. Climate,* **9,** 1959–1990.

Xie, P., and P. A. Arkin, 1997: Global precipitation: A 17-year monthly analysis based on gauge observations, satellite estimates, and numerical model outputs. *Bull. Amer. Meteor. Soc.,* **78,** 2539–2558.

Yasunari, T., 1979: Cloudiness fluctuations associated with the Northern Hemisphere summer monsoon. *J. Meteor. Soc. Japan,* **57,** 227–242.

——, 1980: A quasi-stationary appearance of the 30–40 day period in the cloudiness fluctuations during the summer monsoon over India. *J. Meteor. Soc. Japan,* **58,** 225–229.

Yoo, J.-M., and J. A. Carton, 1988: Outgoing longwave radiation derived rainfall in the tropical Atlantic, with emphasis on 1983–84. *J. Climate,* **1,** 1047–1054.